# SANDIA REPORT

SAND2015-2311
Unlimited Release
Printed March 2015

# Limits to Clutter Cancellation in Multi-Aperture GMTI Data

Armin W. Doerry and Douglas L. Bickel

Prepared by
Sandia National Laboratories
Albuquerque, New Mexico 87185 and Livermore, California 94550

Sandia National Laboratories is a multi-program laboratory managed and operated by Sandia Corporation, a wholly owned subsidiary of Lockheed Martin Corporation, for the U.S. Department of Energy's National Nuclear Security Administration under contract DE-AC04-94AL85000.



Issued by Sandia National Laboratories, operated for the United States Department of Energy by Sandia Corporation.



Available to DOE and DOE contractors from

U.S. Department of Energy
Office of Scientific and Technical Information
P.O. Box 62
Oak Ridge, TN 37831

Telephone: (865) 576-8401
Facsimile: (865) 576-5728
E-Mail: reports@adonis.osti.gov
Online ordering: http://www.osti.gov/bridge

Available to the public from

U.S. Department of Commerce
National Technical Information Service
5285 Port Royal Rd.
Springfield, VA 22161

Telephone: (800) 553-6847
Facsimile: (703) 605-6900
E-Mail: orders@ntis.fedworld.gov
Online order: http://www.ntis.gov/help/ordermethods.asp?loc=7-4-0#online

SAND2015-2311
Unlimited Release
Printed March 2015

# Limits to Clutter Cancellation in Multi-Aperture GMTI Data

Armin W. Doerry
ISR Mission Engineering

Douglas L. Bickel
ISR Analysis & Applications

Sandia National Laboratories
PO Box 5800
Albuquerque, NM 87185-0519

## Abstract

Multi-aperture or multi-subaperture antennas are fundamental to Ground Moving Target Indicator (GMTI) radar systems in order to detect slow-moving targets with Doppler characteristics similar to clutter. Herein we examine the performance of several subaperture architectures for their clutter cancelling performance. Significantly, more antenna phase centers isn't always better, and in fact is sometimes worse, for detecting targets.

## Acknowledgements

This work was supported in part by the Laboratory Directed Research and Development (LDRD) program at Sandia National Laboratories, specifically the “Moving Target Detection and Location in Terrain Using Radar” (158770) LDRD.

This report is also in part the result of an unfunded research and development activity.

Sandia National Laboratories is a multi-program laboratory managed and operated by Sandia Corporation, a wholly owned subsidiary of Lockheed Martin Corporation, for the U.S. Department of Energy’s National Nuclear Security Administration under contract DE-AC04-94AL85000.

# Contents

## Foreword

This report details the results of an academic study. It does not presently exemplify any modes, methodologies, or techniques employed by any operational system known to the author.

## Classification

The specific mathematics and algorithms presented herein do not bear any release restrictions or distribution limitations.

This distribution limitations of this report are in accordance with the classification guidance detailed in the memorandum “Classification Guidance Recommendations for Sandia Radar Testbed Research and Development”, DRAFT memorandum from Brett Remund (Deputy Director, RF Remote Sensing Systems, Electronic Systems Center) to Randy Bell (US Department of Energy, NA-22), February 23, 2004. Sandia has adopted this guidance where otherwise none has been given.

This report formalizes preexisting informal notes and other documentation on the subject matter herein.

# 1 Introduction & Background

The intent of Ground Moving Target Indicator (GMTI) radar is generally to detect and locate targets moving on the ground. A principal indicator of this is the Doppler shift of the target, manifesting as a pulse-to-pulse phase shift of the return echo. Of course, from a moving radar platform, stationary clutter itself will exhibit similar Doppler shifts across a spectrum defined by the antenna beam pattern, the look direction, and the platform's velocity vector.

For slow-moving targets, discriminating the response of a legitimate moving target from the response of otherwise stationary clutter at the same Doppler frequency becomes problematic. The conventional approach to this is to augment Doppler measurements with Direction of Arrival (DOA) measurements from a multi-aperture, or multiple subaperture antenna. Essentially, any pixel for which its DOA doesn't match the DOA corresponding to the stationary clutter element for that particular Doppler frequency is considered moving.

The basic idea then for detecting a moving target is to place a DOA null in the direction of the stationary clutter echo, and then ascribing any sufficient residual energy that 'leaks' through this to a moving target. Of course, a finite antenna aperture width cannot support an arbitrarily narrow notch surrounding the null. Consequently, echo energy from targets that are moving too slowly will also be attenuated by the sidewalls of the DOA notch. We are then clearly interested in "How slow is too slow?" That is "Just how wide are the notches that surround the null?"

A reasonable question for GMTI system design is "What is the nature of the notch that surrounds the null?" Specifically, we desire to understand the relationship of the notch characteristics to other antenna parameters, such as aperture size and number of subapertures, or phase centers. This understanding will then define system performance limits and influence antenna requirements.

We note that in this report, we are more concerned with 'detecting' moving targets, and not necessarily locating them. As a consequence, we are principally interested in the nature of a single DOA notch for the purposes of nulling clutter.

We stipulate that measuring the DOA towards a moving target can be cast as a null-steering problem for a second null. For details, we refer the reader to a companion report by the authors.[1]

## Monopulse Antennas

It is difficult to discuss DOA measurements using multi-aperture or multi-subaperture antennas without addressing monopulse antennas. A bible in the field is a book by Sherman,[2] with a later edition by Sherman and Barton.[3]

While conventional wisdom tends to associate "monopulse" with merely two antenna phase centers (or equivalent) in any one dimension, in fact Sherman clearly advocates a definition taken from the IEEE Standard on Radar Definitions,[4] where monopulse is "A radar technique in which information concerning the angular location of a target is obtained by comparison of signals received in two *or more* [emphasis added] simultaneously antenna beams."

As such, the purist will understand that any multi-aperture, or multi-subaperture, antenna construct may in fact be called a monopulse antenna if the intent is to ascertain DOA from a common pulse or pulses. Consequently, this report does indeed discuss monopulse antennas. Nevertheless, to avoid confusion with the more pedestrian understanding, and with apologies to the purists, we will tend to sometimes employ alternate verbiage to emphasize more general concepts. Even so, we will at other times relate our discussion to more common monopulse terms.

# 2 Simple Notched Pattern

We begin this discussion by making for the moment several simplifying assumptions. These include

- The clutter is absolutely stationary. That is, there is no clutter motion with respect to its location; either translational, rotational, or oscillatory.
- In a range-Doppler map, the clutter direction is perfectly known for each location in the range-Doppler map. This assumption also means that we will not consider adaptive techniques in this report.
- The antenna will have essentially a continuum of elementary phase centers across a finite total aperture. Furthermore, we have access to independently process this continuum of phase centers.
- We desire an antenna (with attendant processing system) that will allow nulling the stationary clutter and allow passage of all echo energy from all moving objects at different DOA, regardless of how close, and regardless of velocity. Of course, we are concerned with line-of-sight velocity.

Consequently, we desire an antenna pattern, whether real or processed, that offers the following characteristics.

1. A true null with zero gain in a programmable (or processed) direction.
2. A 'notch' around the null that is of minimum width, preferably zero-width.
3. A constant-gain in all other directions.

Later, we will modify these or add additional constraints.

## 2.1 The Signum Model

One simple function that meets our criteria and exhibits a zero-width notch around a null is the signum function. This is defined as

$$\operatorname{sgn}(z) = \begin{cases} +1 & \text{for } z > 0 \\ 0 & \text{for } z = 0 \\ -1 & \text{for } z < 0 \end{cases}. \tag{1}$$

We construct an antenna pattern that has a programmable null direction with the function

$$P_{\Delta}\left(\frac{\theta}{\lambda}\right) = -j \operatorname{sgn}\left(\frac{\theta - \theta_0}{\lambda}\right), \tag{2}$$

where

$\theta$ = the independent variable that is the direction of interest,
$\theta_0$ = the direction of the desired null, and
$\lambda$ = nominal wavelength of the signal (positive real value). (3)

We have included the scaling by $-j$ with some malice of forethought.

We recall that the antenna aperture illumination function and the far-field antenna pattern constitute a Fourier Transform pair. Specifically, we identify for a generic pattern

$$P\left(\frac{\theta}{\lambda}\right) = \int p(x) e^{-j2\pi\frac{\theta}{\lambda}x} dx \text{ , and}$$

$$p(x) = \int P\left(\frac{\theta}{\lambda}\right) e^{j2\pi\frac{\theta}{\lambda}x} \frac{d\theta}{\lambda}, \quad (4)$$

where

$p(x)$ = aperture illumination function for a flat or linear aperture, and
$x$ = the independent variable that is the position along the aperture. (5)

We identify this relationship with the shorthand

$$p(x) \Leftrightarrow P\left(\frac{\theta}{\lambda}\right). \quad (6)$$

Purists will note that $\theta$ should really be $\sin\theta$, but for most microwave radar systems, the small angle approximation will suffice.

Accordingly we identify the Fourier Transform pair

$$\frac{1}{\pi x} e^{j2\pi\frac{\theta_0}{\lambda}x} \Leftrightarrow -j\,\mathrm{sgn}\left(\frac{\theta-\theta_0}{\lambda}\right). \quad (7)$$

Consequently, to achieve a far-field antenna pattern as given in Eq. (2), we need an aperture illumination function given by

$$p_\Delta(x) = \frac{1}{\pi x} e^{j2\pi\frac{\theta_0}{\lambda}x}. \quad (8)$$

This aperture illumination function is illustrated in Figure 1.

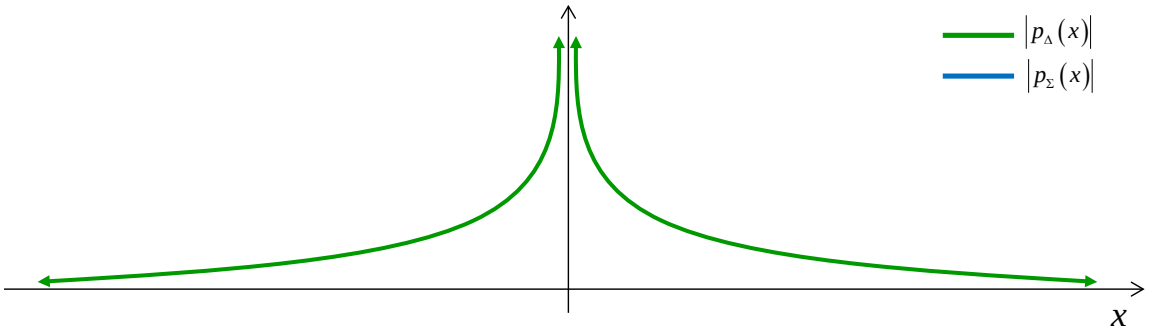


**Figure 1. Aperture illumination for signum model antenna pattern.**

We note several observations.

- This aperture illumination exists for all *x*, except $x = 0$. That is, we require an aperture of infinite extent.
- The null is steered by the phase ramp applied across the aperture.
- Apart from the steering of the null, there is no other phase variation in the aperture illumination function. That is, the shape of the null in the far-field pattern is all about the amplitude distribution across the aperture.
- There is a tacit assumption here that small angle approximations are valid. This is more convenience for us than a significant restriction.

## 2.2 Finite Aperture Effects

Now consider an aperture illumination function of the previous section, but limited to a finite aperture length. Accordingly we now assume an aperture illumination function given by

$$p_\Delta(x) = \frac{1}{\pi x} e^{j2\pi \frac{\theta_0}{\lambda} x} \operatorname{rect}\left(\frac{x}{D}\right), \tag{9}$$

where

$$\operatorname{rect}(z) = \begin{cases} 1 & \text{for } |z| < 1/2 \\ 0 & \text{else} \end{cases}. \tag{10}$$

and

$$D = \text{the linear size of the aperture.} \tag{11}$$

We will make the reasonable assumption that the aperture size is large compared to the wavelength. This is generally consistent with our small angle approximation. That is

$$D >> \lambda . \tag{12}$$

This aperture illumination yields a far-field antenna pattern described by

$$P_{\Delta}\left(\frac{\theta}{\lambda}\right) = -j\,\mathrm{sgn}\left(\frac{\theta-\theta_0}{\lambda}\right) * D\,\mathrm{sinc}\left(\frac{\theta}{\lambda/D}\right), \tag{13}$$

where

$$\mathrm{sinc}(z) = \frac{\sin \pi z}{\pi z}, \tag{14}$$

and in this context the '*' denotes convolution. Note that this sinc function is the far-field pattern for a uniformly illuminated aperture, albeit steered to the null direction, and is often referred to as the 'sum' or 'reference' pattern. Specifically we identify the aperture illumination and sum far-field pattern as

$$p_{\Sigma}(x) = e^{j2\pi\frac{\theta_0}{\lambda}x}\,\mathrm{rect}\left(\frac{x}{D}\right), \text{ and}$$
$$P_{\Sigma}\left(\frac{\theta}{\lambda}\right) = D\,\mathrm{sinc}\left(\frac{\theta-\theta_0}{\lambda/D}\right). \tag{15}$$

These aperture illumination functions are illustrated in Figure 2.

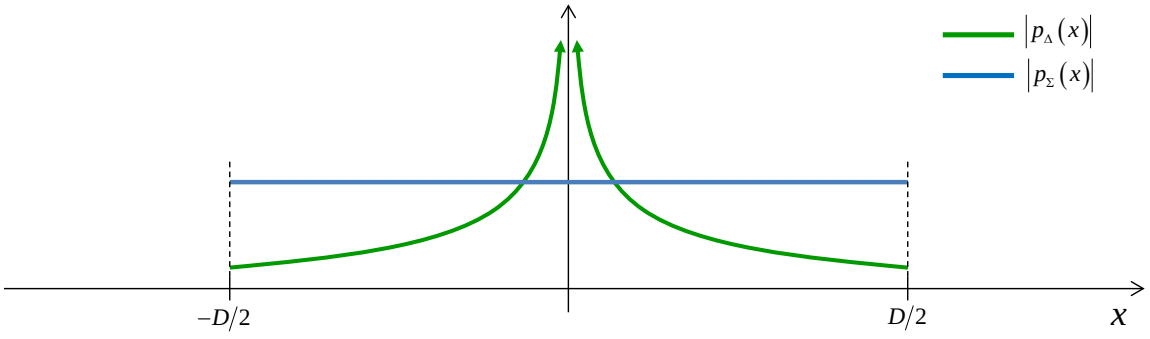


**Figure 2. Aperture illumination for signum model antenna pattern with finite aperture.**

We observe the following.

- The convolution 'smears' the signum function, thereby restricting the rate of change in the far-field pattern as a function of angle.
- The transition region of the signum function has been widened to on the order of the width of the sum pattern mainlobe, namely $\lambda/D$.
- The null still exists, even in the same place as before.
- As a consequence of the widening of the transition region, the notch that surrounds the null has been widened.
- The widening of the notch depends on the total aperture width.
- Since the sum pattern represents the radar's transmitted signal's antenna pattern, we are typically interested only in the region of the mainlobe of the sum pattern.

These features are illustrated in Figure 3. Recall that we have assumed an ideal case and not yet entertained any discrete subapertures.

We state here that for Figure 3 and all subsequent figures, we will identify

$$\theta_{BW} = \lambda/D \text{ = reference beamwidth.} \tag{16}$$

## 2.3 Normalized Notch Pattern

Heretofore we have dealt with far-field patterns that have unit gain. This is typically not the case for real antennas. Furthermore, echo energy will also manifest a two-way antenna pattern and target scene reflectivity fluctuations. Consequently, in practice, the notched pattern response is typically normalized to the sum pattern response. We then identify the normalized notched pattern as

$$P_{\Delta/\Sigma}\left(\frac{\theta}{\lambda}\right) = \frac{P_{\Delta}\left(\frac{\theta}{\lambda}\right) P_{\Sigma}\left(\frac{\theta}{\lambda}\right) \gamma(\theta)}{j\, P_{\Sigma}\left(\frac{\theta}{\lambda}\right) P_{\Sigma}\left(\frac{\theta}{\lambda}\right) \gamma(\theta)}. \tag{17}$$

where

$$\gamma(\theta) \text{ = target reflection response.} \tag{18}$$

The numerator is the two-way notch pattern response from the target scene, and the denominator is the two-way sum pattern response from the target scene. This of course reduces to

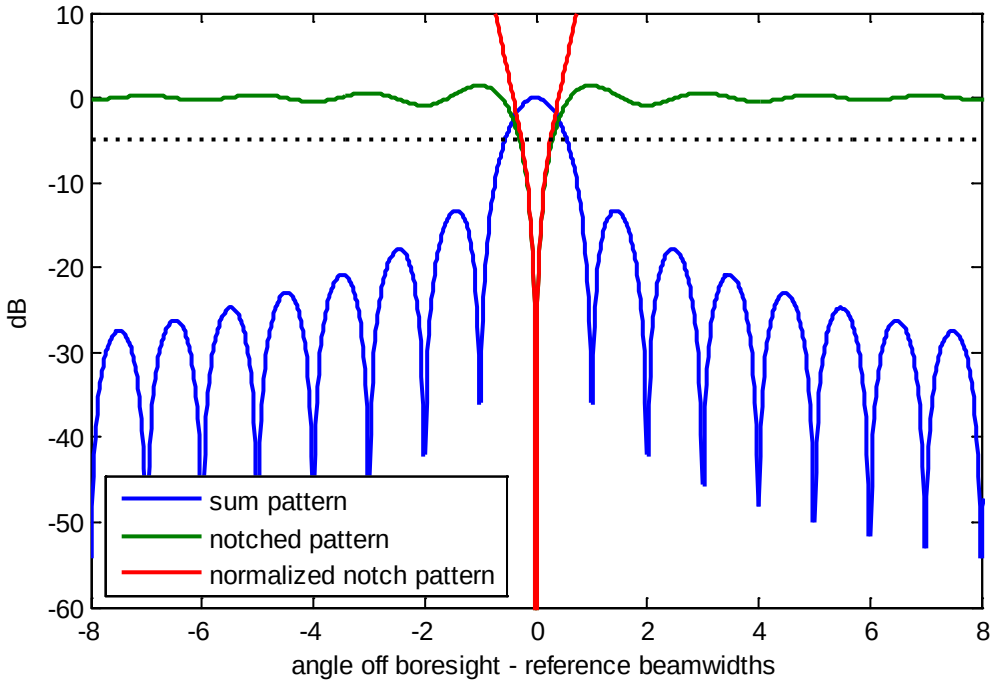


**Figure 3. The far-field pattern of a uniformly illuminated aperture along with the notched pattern given by Eq. (13), and normalized notched pattern given by Eq. (19).**

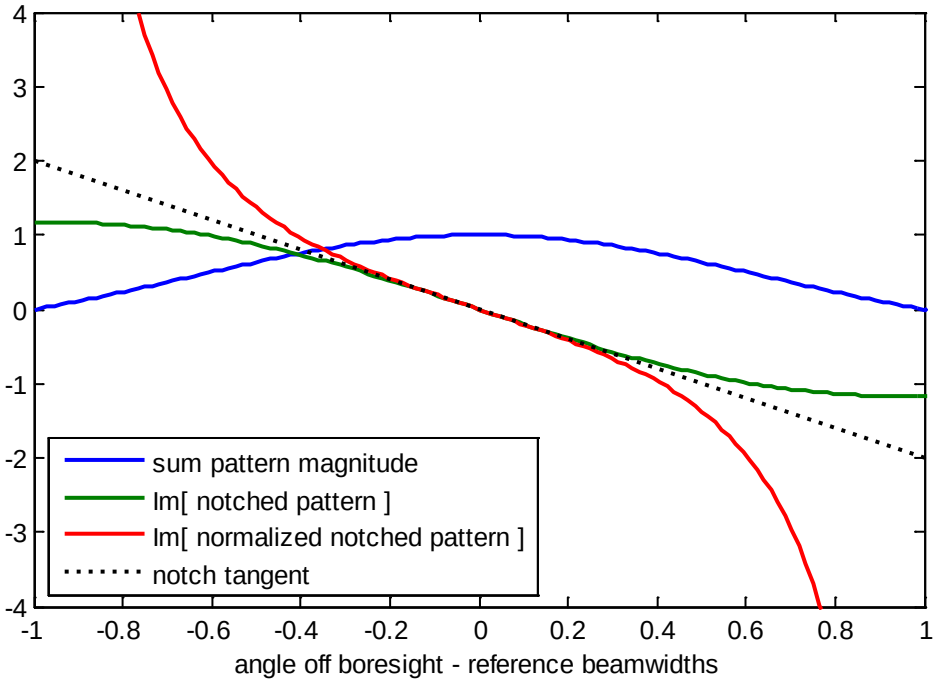


**Figure 4. The far-field patterns of Figure 3 plotted on a linear scale, and zoomed to the region of the mainlobe of the sum pattern.**

$$P_{\Delta/\Sigma}\left(\frac{\theta}{\lambda}\right) = \frac{P_{\Delta}\left(\frac{\theta}{\lambda}\right)}{j\, P_{\Sigma}\left(\frac{\theta}{\lambda}\right)}. \tag{19}$$

The dependence on target scene reflectivity has been eliminated. We recognize that the sum pattern is real-valued and the notch pattern is imaginary (in the sense of a $\pi/2$ phase, and not in the sense of "Puff the magic dragon"). This will hold for the remainder of this report. Consequently, with malice of forethought, we have included a division by *j* to keep this normalized notch pattern real-valued.

We illustrate this normalized notch pattern also in Figure 3. Note that in the central part of the mainlobe of the sum pattern, the normalized notch pattern essentially tracks the unit gain notch pattern.

In monopulse radar literature, the normalized notch pattern is typically referred to as the "normalized error signal" or "normalized difference signal."

## 2.4 Notch Width

It is difficult to discuss the width of the notch without some specific measure or metric for the notch width. A somewhat arbitrary but nevertheless common measure for multi-aperture GMTI processing is the width of the notch in the notched spectrum as measured at –5 dB with respect to the far-field sum pattern peak.[5, 6] We note that a reduction of 5 dB in receiver antenna gain for a monostatic radar exhibiting a quartic range dependence requires a 25% range reduction to maintain Signal-to-Noise Ratio (SNR).

Herein we will also adopt this measure.

Such a measure might be considered the resolution of the null, analogous to the more familiar resolution of a peak response.

The –5 dB line is also illustrated in Figure 3. We note that the –5 dB notch width (scaled to unit sum pattern mainlobe width) is 0.59. Perhaps also of interest is that the notch width in the normalized notch pattern, that is the "normalized notch width," is 0.52.

## 2.5 Notch Pattern Slope

Not easily appreciated with the 'dB' scale in Figure 3 is the nature of the slope of the notch. Consequently we re-plot elements of Figure 3 on a linear scale in Figure 4.

We make some observations here.

- We note in particular that the normalized notch pattern, as well as the notch pattern itself (scaled to unit gain and unit reference beamwidth), exhibit a slope of $-2$ at the center of the sum pattern, in the vicinity of the null.
- Furthermore, the slope is monotonic and reasonably linear for a large portion of the sum pattern mainlobe width.
- The notch slope is in fact a measure of how narrow is the notch. A steeper slope corresponds to a narrower notch.
- By measuring the value of the ratio of notch pattern response to sum pattern response, we can effectively determine the angular offset from boresight of a target echo signal, regardless of its reflectivity. The steeper is the slope, the more sensitive we are to angular offsets.
- In monopulse antenna literature, this notch slope is identically the well-known monopulse slope of the antenna.

## 2.6 Some Comments

While we have met our stated design criteria for a notched antenna pattern, we nevertheless face some serious issues with this particular construct. We offer the following observations.

- The aperture illumination function for the notched pattern $p_{\Delta}(x)$ contains a $1/x$ taper characteristic that is not realistic to generate.
- A real antenna will ultimately have a limited effective area. This in turn places a limit on maximum achievable gain, which in turn places a finite limit on the area under the curve given by $\left|p_{\Delta}(x)\right|$. The given $p_{\Delta}(x)$ does not meet this constraint.
- Further analysis of the aperture illumination function reveals that the width of the notch is principally a function of the aperture diameter $D$, indicating that it is the 'outside' parts of the illuminated aperture that contribute most to the far-field pattern notch width.
- Further analysis of the aperture illumination function also reveals that it is the $1/x$ taper characteristic towards the center of the aperture is principally involved with the role of a uniform magnitude far-field pattern away from the notch.
- Our constraint for the notched pattern has been to attempt a constant non-zero response to all angles except in the direction of the null. As a practical matter, for a monostatic antenna there is no need to achieve this response for directions outside of the main beam of the sum pattern. Consequently this over-constrains our design, and potentially adversely affects the achievable notch width.

# 3 Constrained Aperture for Notched Pattern

We now modify our design criteria for a notched antenna pattern to embody the following characteristics.

1. A true null with zero gain in a programmable (or processed) direction.
2. A 'notch' around the null that is of minimum width, preferably zero-width.
3. A gain in other directions that is as near to unity as possible within the neighborhood of the sum pattern mainlobe, subject to the constraint on the notched pattern aperture illumination function as follows.

$$\int_{-\infty}^{\infty} \left| p_{\Delta}(x) \right| dx = \int_{-\infty}^{\infty} \left| p_{\Sigma}(x) \right| dx \tag{20}$$

This is a necessary constraint for a limited-gain antenna, where sum pattern aperture is the same effective size as the notched pattern aperture. We do not quibble about whether we can introduce a constant relative scale factor in this equation. The point is that the apertures need to be finite and this suffices for our thought experiment.

Recall from the last section that it is the outside of the aperture that contributes the most to narrowing the notch width. Consequently we take a cue from the interferometry body of knowledge, and choose the aperture illumination function for the notched far-field pattern as

$$p_{\Delta}(x) = \operatorname{sgn}(x) e^{j2\pi \frac{\theta_0}{\lambda} x} \left[ \frac{D}{2} \delta\left( x - \frac{D}{2} \right) + \frac{D}{2} \delta\left( x + \frac{D}{2} \right) \right], \tag{21}$$

where

$$\delta(z) = \text{Dirac delta function.} \tag{22}$$

This aperture illumination yields a far-field antenna pattern described by

$$P_{\Delta}\left( \frac{\theta}{\lambda} \right) = -jD \sin\left( \pi \frac{\theta - \theta_0}{\theta_{BW}} \right). \tag{23}$$

We will examine two different sum or reference patterns.

## 3.1 Most Narrow Sum Pattern

The first sum pattern we describe essentially uses the same phase centers as the notched pattern's aperture illumination function. That is, we define and identify the aperture illumination function and its far-field pattern as

$$p_{\Sigma}(x) = e^{j2\pi\frac{\theta_0}{\lambda}x}\left[\frac{D}{2}\delta\left(x-\frac{D}{2}\right)+\frac{D}{2}\delta\left(x+\frac{D}{2}\right)\right], \text{ and}$$

$$P_{\Sigma}\left(\frac{\theta}{\lambda}\right) = D\cos\left(\pi\frac{\theta-\theta_0}{\theta_{BW}}\right). \tag{24}$$

The normalized notched pattern is then described by

$$P_{\Delta/\Sigma}\left(\frac{\theta}{\lambda}\right) = \frac{P_{\Delta}\left(\frac{\theta}{\lambda}\right)}{j\,P_{\Sigma}\left(\frac{\theta}{\lambda}\right)} = \frac{-D\sin\left(\pi\frac{\theta-\theta_0}{\theta_{BW}}\right)}{D\cos\left(\pi\frac{\theta-\theta_0}{\theta_{BW}}\right)}. \tag{25}$$

This can be further simplified to

$$P_{\Delta/\Sigma}\left(\frac{\theta}{\lambda}\right) = -\tan\left(\pi\frac{\theta-\theta_0}{\theta_{BW}}\right). \tag{26}$$

The aperture illumination functions are illustrated in Figure 5. The corresponding patterns are shown in Figure 6 and Figure 7.

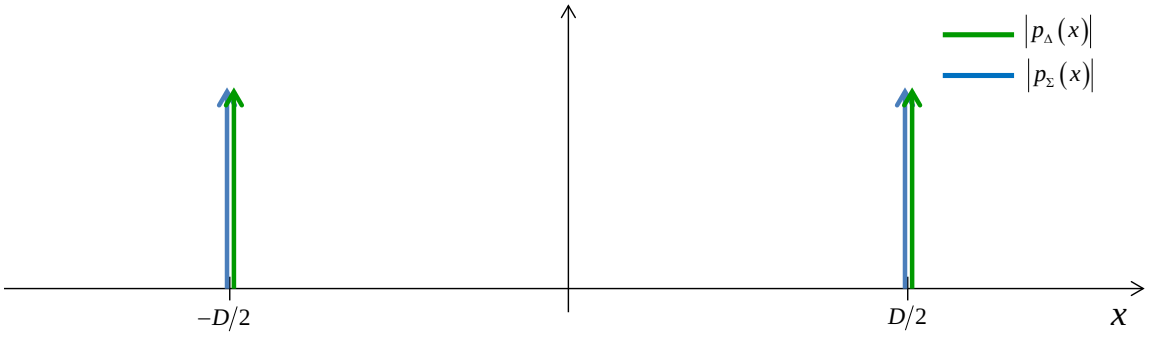


**Figure 5. Aperture illumination for impulse response sum and delta channels.**

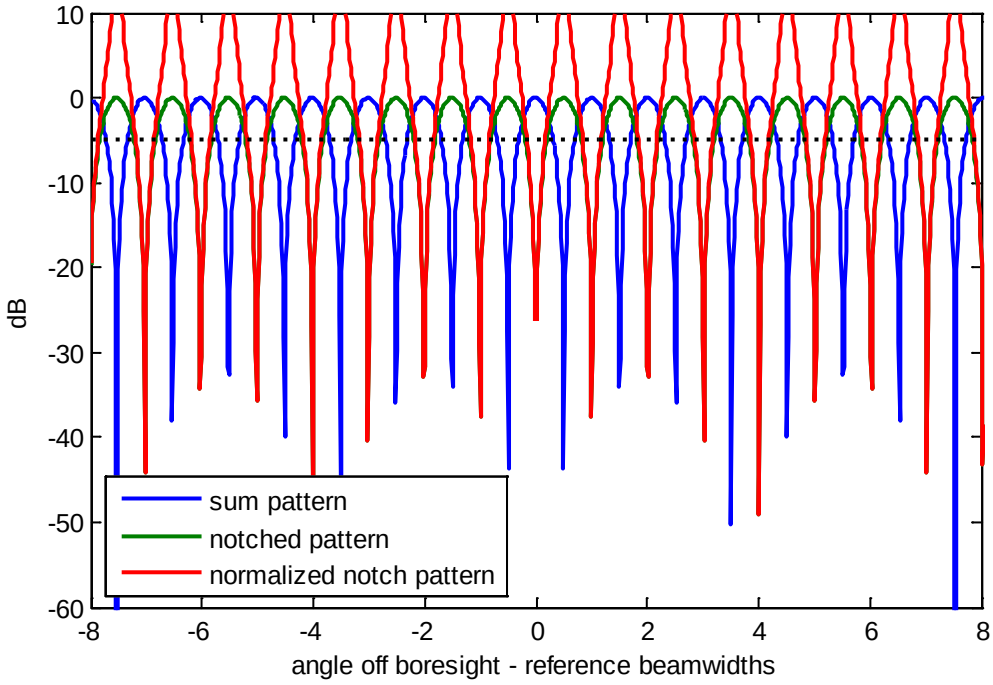


**Figure 6. The far-field sum pattern of a dual-impulse aperture along with the notched pattern given by Eq. (23), and normalized notched pattern given by Eq. (26).**

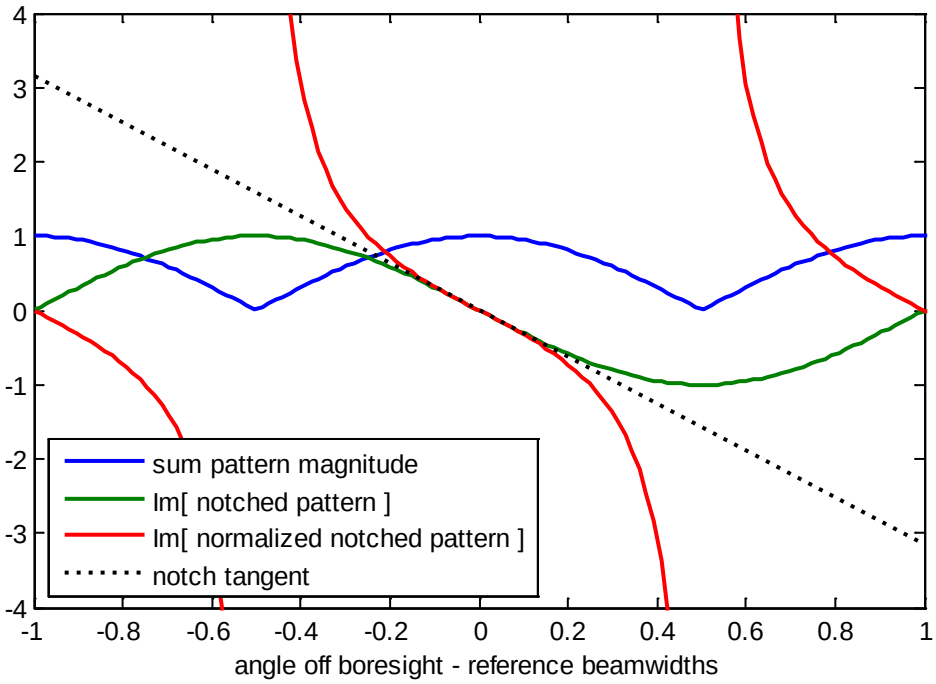


**Figure 7. The far-field patterns of Figure 6 plotted on a linear scale, and zoomed to the region of the mainlobe of the sum pattern.**

We make the following observations.

- The normalized notch pattern, as well as the notch pattern itself (scaled to equivalent gain and unit reference beamwidth), exhibit a normalized monopulse slope of $-\pi$ at the center of the sum pattern, in the vicinity of the null.
- This is a steeper notch slope than in the previous section.
- The –5 dB notch width is 0.38, with normalized notch width of 0.33.
- The aperture illumination function for both the sum pattern $p_\Sigma(x)$ and notched pattern $p_\Delta(x)$ contain two omnidirectional impulse functions.
- The impulse nature of both far-field patterns generates grating lobes that yield ambiguous directional responses. This isn't so good, and a common problem of interferometers.

## 3.2 Uniform Sum Pattern

We now return to a sum pattern described by a uniformly illuminated aperture. That is, we define and identify the aperture illumination function and its far-field pattern as

$$p_\Sigma(x) = e^{j2\pi\frac{\theta_0}{\lambda}x}\,\mathrm{rect}\left(\frac{x}{D}\right), \text{ and}$$
$$P_\Sigma\left(\frac{\theta}{\lambda}\right) = D\,\mathrm{sinc}\left(\frac{\theta-\theta_0}{\theta_{BW}}\right). \tag{27}$$

The normalized notched pattern is then described by

$$P_{\Delta/\Sigma}\left(\frac{\theta}{\lambda}\right) = \frac{P_\Delta\left(\frac{\theta}{\lambda}\right)}{j\,P_\Sigma\left(\frac{\theta}{\lambda}\right)} = \frac{-\sin\left(\pi\frac{\theta-\theta_0}{\theta_{BW}}\right)}{\mathrm{sinc}\left(\frac{\theta-\theta_0}{\theta_{BW}}\right)}. \tag{28}$$

This can be further simplified to

$$P_{\Delta/\Sigma}\left(\frac{\theta}{\lambda}\right) = -\pi\left(\frac{\theta-\theta_0}{\theta_{BW}}\right), \tag{29}$$

although we recognize some difficulties in the immediate neighborhood of the nulls.

The aperture illumination functions are illustrated in Figure 8. The corresponding patterns are shown in Figure 9 and Figure 10.

We make the following observations.

- The normalized notch pattern, as well as the notch pattern itself (scaled to equivalent gain and unit reference beamwidth), exhibit a normalized monopulse slope of $-\pi$ at the center of the sum pattern, in the vicinity of the null. Interestingly, this slope is exactly linear well beyond the nominal beamwidth of the sum pattern.
- This is still a steeper notch slope than in the previous section.
- Only the aperture illumination function for the notched pattern $p_\Delta(x)$ contains two impulse functions. While we can probably conjure some architectures where this is approachable, the taper characteristic is probably still not all that realistic to generate.
- The –5 dB notch width is still 0.38, with normalized notch width of 0.36.

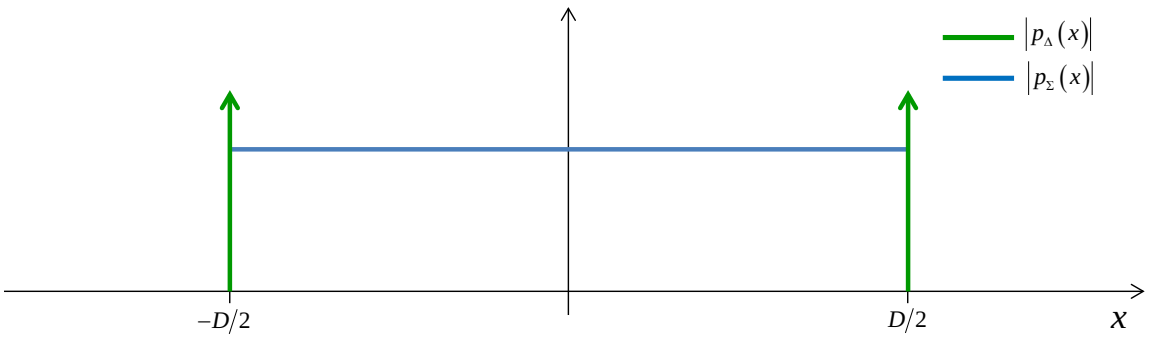


**Figure 8. Aperture illumination for impulse response delta channel and uniform sum channel.**

## 3.3 Some Comments

We offer the following observations.

- For the architectures considered, the notch width is purely a function of the notched pattern's aperture illumination.
- The sum pattern merely serves to select a particular portion of the notched pattern as significant.

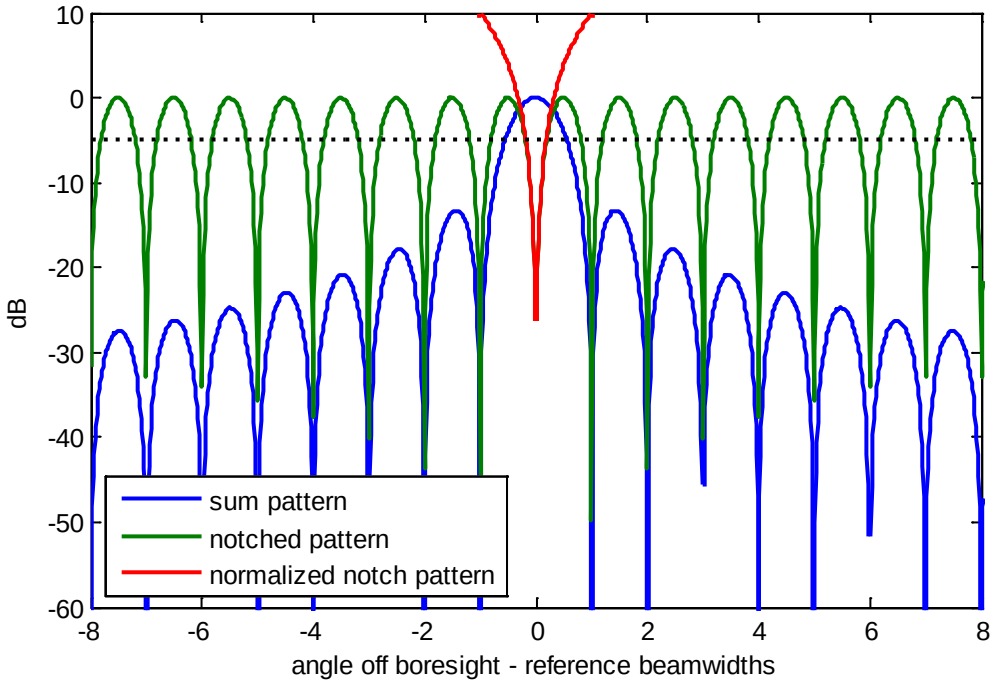


**Figure 9. The far-field pattern of a uniformly illuminated aperture along with the notched pattern given by Eq. (23), and normalized notched pattern given by Eq. (29).**

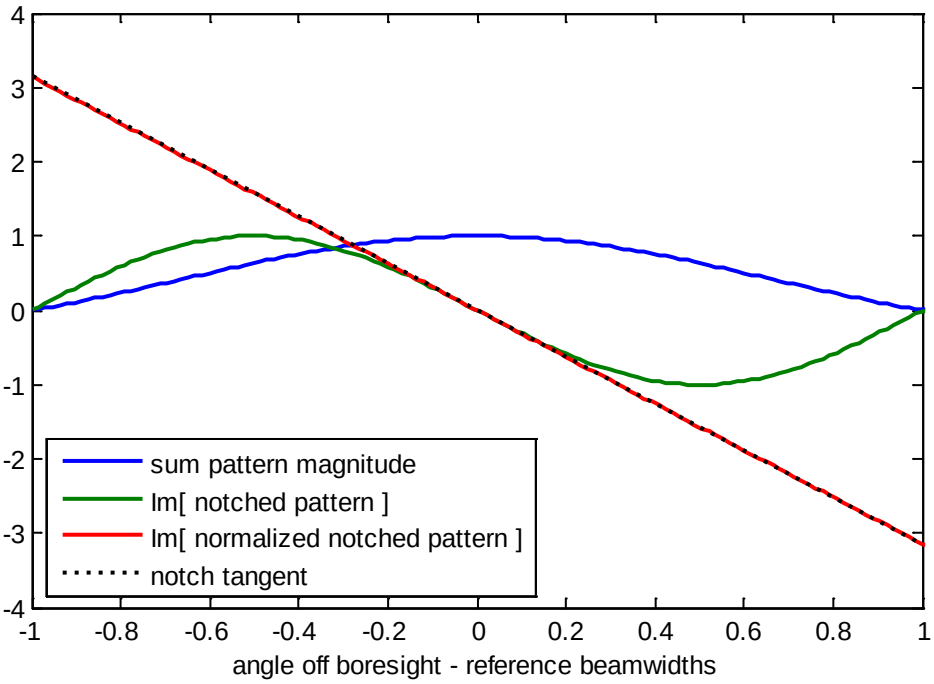


**Figure 10. The far-field patterns of Figure 9 plotted on a linear scale, and zoomed to the region of the mainlobe of the sum pattern.**

# 4 Continuous Uniform (Non-Tapered) Aperture

We now modify our design criteria for a notched antenna pattern to embody the following characteristics.

1. A true null with zero gain in a programmable (or processed) direction.
2. A 'notch' around the null that is of minimum width.
3. A gain in other directions that is as near to unity as possible within the neighborhood of the sum pattern mainlobe, subject to the constraint on the notched pattern aperture illumination function as follows, at least in the limit.

$$\left|p_{\Delta}(x)\right| = \left|p_{\Sigma}(x)\right| = \text{rect}\left(\frac{x}{D}\right). \tag{30}$$

Here we constrain that any one elemental position in the sum pattern aperture exhibits the same magnitude gain as the respective elemental position in the notched pattern aperture. The only difference is in the phase between the two apertures.

Consequently we identify the aperture illumination function for the notched far-field pattern as

$$p_{\Delta}(x) = \text{sgn}(x) e^{j2\pi\frac{\theta_0}{\lambda}x} \text{rect}\left(\frac{x}{D}\right). \tag{31}$$

We observe that this meets the constraint of Eq. (30) except strictly at $x = 0$. However, in the limit the constraint does hold. This aperture illumination yields a far-field antenna pattern described by

$$P_{\Delta}\left(\frac{\theta}{\lambda}\right) = \frac{-j}{\pi\left(\frac{\theta-\theta_0}{\lambda}\right)} * D\,\text{sinc}\left(\frac{\theta}{\theta_{BW}}\right). \tag{32}$$

This can be calculated to the closed-form given by

$$P_{\Delta}\left(\frac{\theta}{\lambda}\right) = -jD\left(\frac{1-\cos\left(\pi\left(\frac{\theta-\theta_0}{\theta_{BW}}\right)\right)}{\pi\left(\frac{\theta-\theta_0}{\theta_{BW}}\right)}\right). \tag{33}$$

The sum pattern remains described by

$$p_\Sigma(x) = e^{j2\pi\frac{\theta_0}{\lambda}x}\,\mathrm{rect}\left(\frac{x}{D}\right), \text{ and}$$

$$P_\Sigma\left(\frac{\theta}{\lambda}\right) = D\,\mathrm{sinc}\left(\frac{\theta-\theta_0}{\theta_{BW}}\right). \tag{34}$$

The attractiveness here is that each antenna elemental position in the respective apertures has the same magnitude gain, and differs between sum and notch patterns only in phase.

The normalized notched pattern is calculated to be

$$P_{\Delta/\Sigma}\left(\frac{\theta}{\lambda}\right) = \frac{P_\Delta\left(\frac{\theta}{\lambda}\right)}{j\,P_\Sigma\left(\frac{\theta}{\lambda}\right)} = -\left(\frac{1-\cos\left(\pi\left(\frac{\theta-\theta_0}{\theta_{BW}}\right)\right)}{\sin\left(\pi\left(\frac{\theta-\theta_0}{\theta_{BW}}\right)\right)}\right), \tag{35}$$

The aperture illumination functions are illustrated in Figure 11. The corresponding antenna pattern plots are given in Figure 12 and Figure 13.

We make the following observations.

- The normalized notch pattern, as well as the notch pattern itself (scaled to equivalent gain and unit reference beamwidth), exhibits a normalized monopulse slope of $-(\pi/2)$ at the center of the sum pattern, in the vicinity of the null.
- This is a less steep notch slope than in any of the previous sections.
- The –5 dB notch width is 0.83, with normalized notch width of 0.65.
- This aperture illumination function for the notched pattern $p_\Delta(x)$ is, however, quite realistic to generate.

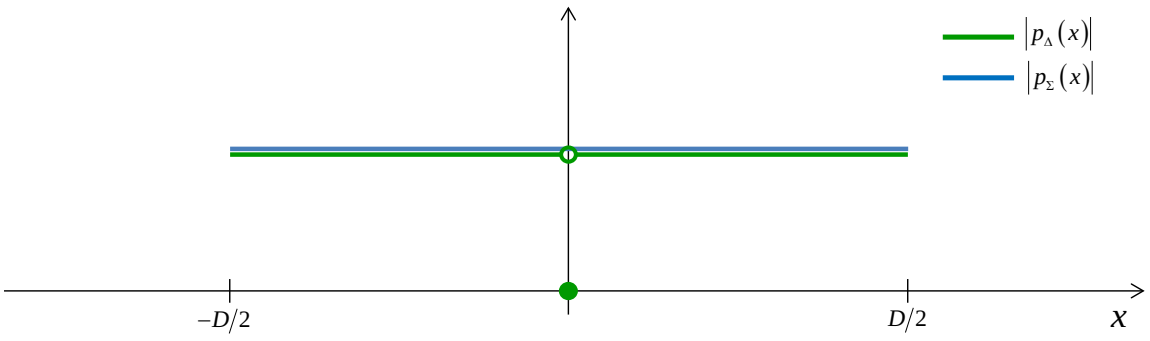


**Figure 11. Aperture illumination for uniform delta channel and uniform sum channel.**

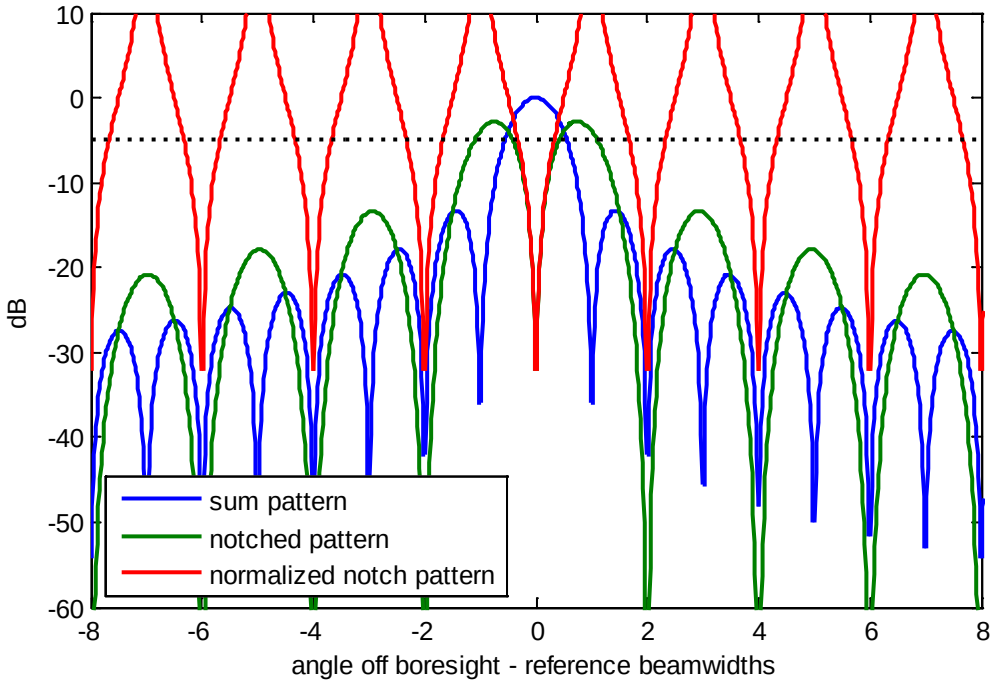


**Figure 12. The far-field pattern of a uniformly illuminated aperture along with the notched pattern given by Eq. (32), and normalized notched pattern given by Eq. (35).**

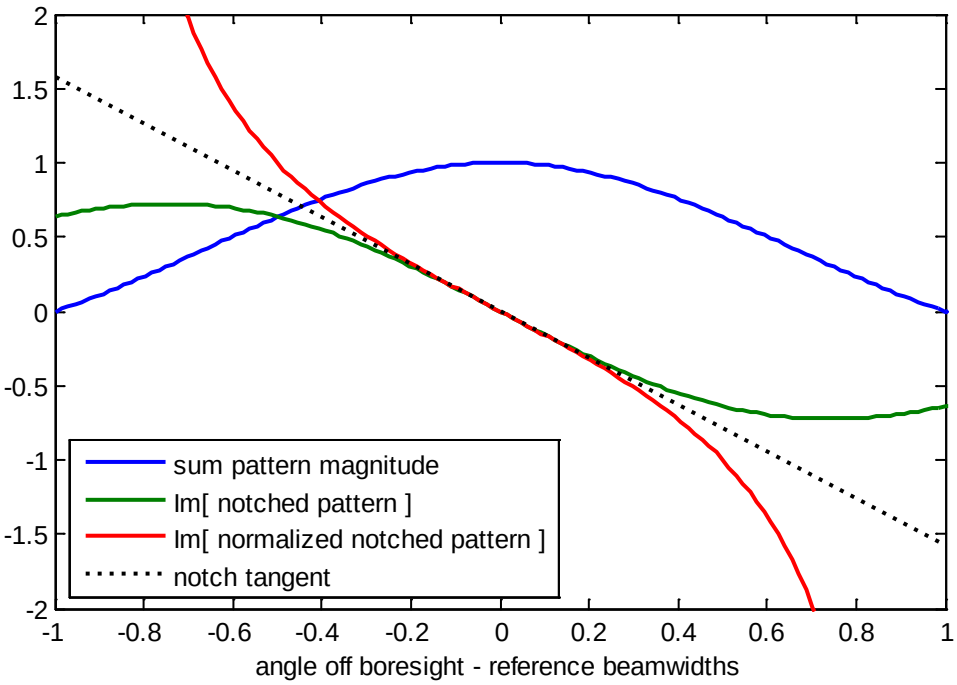


**Figure 13. The far-field patterns of Figure 12 plotted on a linear scale, and zoomed to the region of the mainlobe of the sum pattern.**

*“Out of clutter, find simplicity.” ― Albert Einstein*

# 5 Sampled Uniform Aperture

We now modify our design criteria for a notched antenna pattern to embody the following characteristics.

1. A true null with zero gain in a programmable (or processed) direction.
2. A 'notch' around the null that is of minimum width.
3. A gain in other directions that is as near to unity as possible within the neighborhood of the sum pattern mainlobe, subject to the constraint on the aperture illumination functions that they are a set of equally-spaced and equal-area samples as follows.

$$\left|p_{\Delta}(x)\right| = \left|p_{\Sigma}(x)\right| = \frac{1}{N}\sum_{n=0}^{N-1}\delta(x - x_n), \tag{36}$$

except perhaps at $x = 0$. Here, $x_n$ are the sample positions in the overall aperture.

Here we also constrain that any one elemental position in the sum pattern aperture exhibits the same magnitude gain as the respective elemental position in the notched pattern aperture, except perhaps at $x = 0$. The phase between the two apertures may be significantly different. The desire is to investigate a sampled version of the aperture illuminations described in the previous section. Accordingly, we define the sample positions as

$$x_n = \frac{D}{N}n - \frac{D}{N}\left(\frac{N-1}{2}\right), \tag{37}$$

where the sample indexed positions are identified

$$n \in \textit{Integers}, \text{ where } 0 \le n < N. \tag{38}$$

We define the aperture illumination functions as

$$p_{\Delta}(x) = \frac{1}{N}\sum_{n=0}^{N-1}\operatorname{sgn}(x)e^{j2\pi\frac{\theta_0}{\lambda}x}\delta\left(x - \frac{D}{N}n + \frac{D}{N}\left(\frac{N-1}{2}\right)\right), \text{ and}$$

$$p_{\Sigma}(x) = \frac{1}{N}\sum_{n=0}^{N-1}e^{j2\pi\frac{\theta_0}{\lambda}x}\delta\left(x - \frac{D}{N}n + \frac{D}{N}\left(\frac{N-1}{2}\right)\right). \tag{39}$$

Note that we have placed the samples in the center of equal-length segments formed by dividing the larger aperture into subapertures. For convenience, we will separately analyze the case of an even number of samples from the case of an odd number of samples.

## 5.1 Even Number of Samples

We now concern ourselves with only even values of *N*. We repeat and slightly expand the aperture illumination functions as

$$p_{\Delta}(x) = \begin{bmatrix} -\frac{1}{N}\sum_{n=0}^{N/2-1} e^{j2\pi\frac{\theta_0}{\lambda}x}\delta\left(x - \frac{D}{N}n + \frac{D}{N}\left(\frac{N-1}{2}\right)\right) \\ +\frac{1}{N}\sum_{n=N/2}^{N-1} e^{j2\pi\frac{\theta_0}{\lambda}x}\delta\left(x - \frac{D}{N}n + \frac{D}{N}\left(\frac{N-1}{2}\right)\right) \end{bmatrix}, \text{ and}$$

$$p_{\Sigma}(x) = \frac{1}{N}\sum_{n=0}^{N-1} e^{j2\pi\frac{\theta_0}{\lambda}x}\delta\left(x - \frac{D}{N}n + \frac{D}{N}\left(\frac{N-1}{2}\right)\right). \tag{40}$$

The corresponding antenna patterns can then be calculated as

$$P_{\Delta}\left(\frac{\theta}{\lambda}\right) = -\frac{1}{N}e^{j2\pi\left(\frac{\theta-\theta_0}{\lambda}\right)\frac{D}{N}\left(\frac{N-1}{2}\right)}\begin{bmatrix} \sum_{n=0}^{N/2-1} e^{-j2\pi\left(\frac{\theta-\theta_0}{\lambda}\right)\left(\frac{D}{N}\right)n} \\ -\sum_{n=N/2}^{N-1} e^{-j2\pi\left(\frac{\theta-\theta_0}{\lambda}\right)\left(\frac{D}{N}\right)n} \end{bmatrix}, \text{ and}$$

$$P_{\Sigma}\left(\frac{\theta}{\lambda}\right) = \frac{1}{N}e^{j2\pi\left(\frac{\theta-\theta_0}{\lambda}\right)\frac{D}{N}\left(\frac{N-1}{2}\right)}\sum_{n=0}^{N-1} e^{-j2\pi\left(\frac{\theta-\theta_0}{\lambda}\right)\left(\frac{D}{N}\right)n}. \tag{41}$$

Closed form expressions are calculated as, and simplified to

$$P_{\Delta}\left(\frac{\theta}{\lambda}\right) = \frac{-j2}{N}\left(\frac{\sin^2\left(\pi\left(\frac{\theta-\theta_0}{\theta_{BW}}\right)\frac{1}{2}\right)}{\sin\left(\pi\left(\frac{\theta-\theta_0}{\theta_{BW}}\right)\left(\frac{1}{N}\right)\right)}\right) = \frac{-j}{N}\left(\frac{1-\cos\left(\pi\left(\frac{\theta-\theta_0}{\theta_{BW}}\right)\right)}{\sin\left(\pi\left(\frac{\theta-\theta_0}{\theta_{BW}}\right)\left(\frac{1}{N}\right)\right)}\right),$$

and

$$P_{\Sigma}\left(\frac{\theta}{\lambda}\right) = \frac{1}{N}\left(\frac{\sin\left(\pi\left(\frac{\theta-\theta_0}{\theta_{BW}}\right)\right)}{\sin\left(\pi\left(\frac{\theta-\theta_0}{\theta_{BW}}\right)\left(\frac{1}{N}\right)\right)}\right). \tag{42}$$

We have made use of the closed form expression for a power series given as

$$\sum_{n=N_1}^{N_2} z^n = \frac{z^{N_1} - z^{N_2}}{1-z}. \tag{43}$$

The normalized pattern is calculated as

$$P_{\Delta/\Sigma}\left(\frac{\theta}{\lambda}\right) = \frac{P_\Delta\left(\frac{\theta}{\lambda}\right)}{jP_\Sigma\left(\frac{\theta}{\lambda}\right)} = -\left(\frac{1-\cos\left(\pi\left(\frac{\theta-\theta_0}{\theta_{BW}}\right)\right)}{\sin\left(\pi\left(\frac{\theta-\theta_0}{\theta_{BW}}\right)\right)}\right). \tag{44}$$

The aperture illumination functions for $N = 4$ are illustrated in Figure 14. The corresponding antenna pattern plots are given in Figure 15 and Figure 16.

We make the following observations.

- The normalized notch pattern, as well as the notch pattern itself (scaled to equivalent gain and unit reference beamwidth), exhibits a normalized monopulse slope of $-(\pi/2)$ at the center of the sum pattern, in the vicinity of the null.
- This is essentially the same as the continuous uniform aperture. The differences due to the sampled nature of the aperture are small.
- The –5 dB notch width is 0.81, with normalized notch width of 0.65.
- This aperture illumination function, although itself not realistic, does to first order approximate a multi-aperture antenna with four phase centers, where the impulse locations are the independent phase centers.

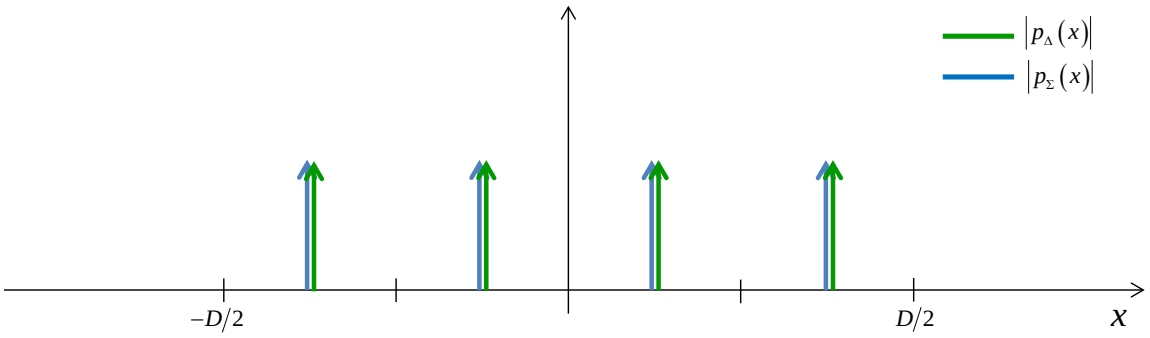


**Figure 14. Aperture illumination for uniform sampled delta and sum channels.**

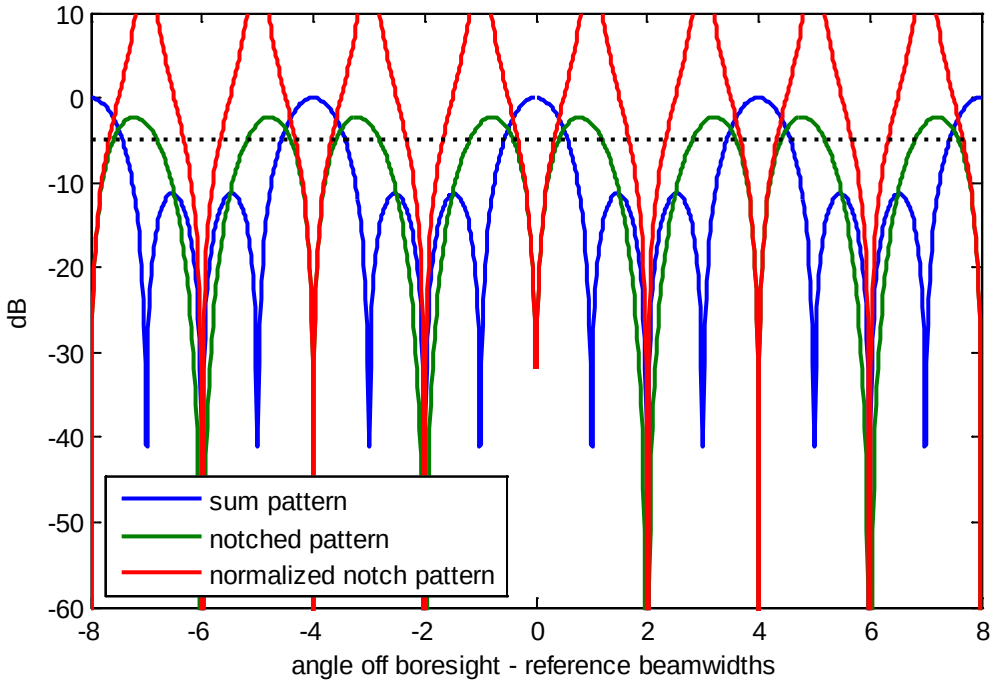


**Figure 15. The far-field pattern of a uniformly sampled aperture along with the notched pattern given by Eq. (42), and normalized notched pattern given by Eq. (44).**

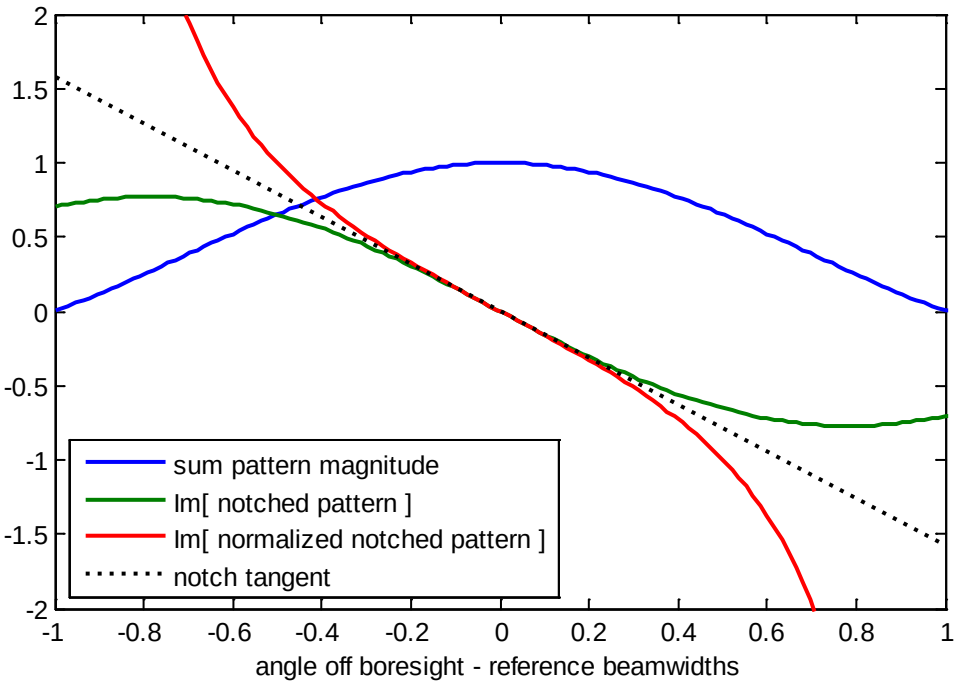


**Figure 16. The far-field patterns of Figure 15 plotted on a linear scale, and zoomed to the region of the mainlobe of the sum pattern.**

## 5.2 Odd Number of Samples

We now concern ourselves with only odd values of *N*. We note that with an odd number of samples, that the center sample falls at the center of the aperture, and will be nulled by the signum function in the notched pattern aperture illumination function. The sum pattern aperture illumination function analysis is otherwise unaffected by even versus odd number of samples, so we will repeat it here for completeness. Consequently, we repeat and slightly expand the aperture illumination functions as

$$p_{\Delta}(x)=\left[\begin{array}{l}-\frac{1}{N}\sum_{n=0}^{(N/2-3/2)}e^{j2\pi\frac{\theta_0}{\lambda}x}\delta\left(x-\frac{D}{N}n+\frac{D}{N}\left(\frac{N-1}{2}\right)\right)\\ +\frac{1}{N}\sum_{n=(N/2+1/2)}^{N-1}e^{j2\pi\frac{\theta_0}{\lambda}x}\delta\left(x-\frac{D}{N}n+\frac{D}{N}\left(\frac{N-1}{2}\right)\right)\end{array}\right], \text{ and}$$

$$p_{\Sigma}(x)=\frac{1}{N}\sum_{n=0}^{N-1}e^{j2\pi\frac{\theta_0}{\lambda}x}\delta\left(x-\frac{D}{N}n+\frac{D}{N}\left(\frac{N-1}{2}\right)\right). \tag{45}$$

The corresponding antenna patterns can then be calculated as

$$P_{\Delta}\left(\frac{\theta}{\lambda}\right)=-\frac{1}{N}e^{j2\pi\left(\frac{\theta-\theta_0}{\lambda}\right)\frac{D}{N}\left(\frac{N-1}{2}\right)}\left[\begin{array}{l}\sum_{n=0}^{(N/2-3/2)}e^{-j2\pi\left(\frac{\theta-\theta_0}{\lambda}\right)\left(\frac{D}{N}\right)n}\\ -\sum_{n=(N/2+1/2)}^{N-1}e^{-j2\pi\left(\frac{\theta-\theta_0}{\lambda}\right)\left(\frac{D}{N}\right)n}\end{array}\right], \text{ and}$$

$$P_{\Sigma}\left(\frac{\theta}{\lambda}\right)=\frac{1}{N}e^{j2\pi\left(\frac{\theta-\theta_0}{\lambda}\right)\frac{D}{N}\left(\frac{N-1}{2}\right)}\sum_{n=0}^{N-1}e^{-j2\pi\left(\frac{\theta-\theta_0}{\lambda}\right)\left(\frac{D}{N}\right)n}. \tag{46}$$

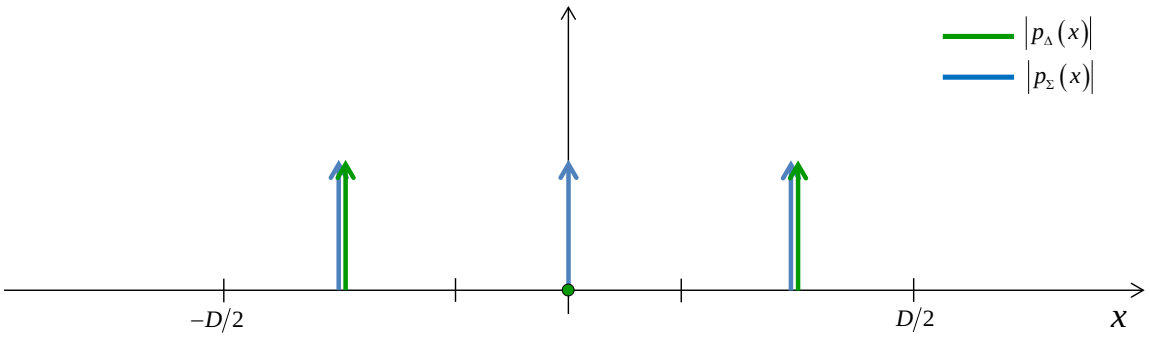


**Figure 17. Aperture illumination for uniform sampled delta and sum channels.**

Closed form expressions are calculated as, and simplified to

$$P_{\Delta}\left(\frac{\theta}{\lambda}\right)=\frac{-j2}{N}\left(\frac{\sin\left(\pi\left(\frac{\theta-\theta_0}{\theta_{BW}}\right)\left(\frac{N-1}{2N}\right)\right)\sin\left(\pi\left(\frac{\theta-\theta_0}{\theta_{BW}}\right)\left(\frac{N+1}{2N}\right)\right)}{\sin\left(\pi\left(\frac{\theta-\theta_0}{\theta_{BW}}\right)\left(\frac{1}{N}\right)\right)}\right),$$

$$=\frac{-j}{N}\left(\frac{\cos\left(\pi\left(\frac{\theta-\theta_0}{\theta_{BW}}\right)\left(\frac{1}{N}\right)\right)-\cos\left(\pi\left(\frac{\theta-\theta_0}{\theta_{BW}}\right)\right)}{\sin\left(\pi\left(\frac{\theta-\theta_0}{\theta_{BW}}\right)\left(\frac{1}{N}\right)\right)}\right),$$

$$P_{\Sigma}\left(\frac{\theta}{\lambda}\right)=\frac{1}{N}\left(\frac{\sin\left(\pi\left(\frac{\theta-\theta_0}{\theta_{BW}}\right)\right)}{\sin\left(\pi\left(\frac{\theta-\theta_0}{\theta_{BW}}\right)\left(\frac{1}{N}\right)\right)}\right). \tag{47}$$

The normalized pattern is calculated as

$$P_{\Delta/\Sigma}\left(\frac{\theta}{\lambda}\right)=\frac{P_{\Delta}\left(\frac{\theta}{\lambda}\right)}{jP_{\Sigma}\left(\frac{\theta}{\lambda}\right)}=-\left(\frac{\cos\left(\pi\left(\frac{\theta-\theta_0}{\theta_{BW}}\right)\left(\frac{1}{N}\right)\right)-\cos\left(\pi\left(\frac{\theta-\theta_0}{\theta_{BW}}\right)\right)}{\sin\left(\pi\left(\frac{\theta-\theta_0}{\theta_{BW}}\right)\right)}\right). \tag{48}$$

The aperture illumination functions for $N=3$ are illustrated in Figure 17. The corresponding antenna pattern plots are given in Figure 18 and Figure 19.

We make the following observations.

- The notched pattern for an odd number of samples approaches that for an even number of samples as *N* increases.
- The normalized notch pattern, as well as the notch pattern itself (scaled to equivalent gain and unit reference beamwidth), exhibits a normalized monopulse slope of something less than $-(\pi/2)$ at the center of the sum pattern, in the vicinity of the null. This is because of the null at $x=0$.
- The –5 dB notch width is 0.96, with normalized notch width of 0.73.
- This aperture illumination function, although itself not realistic, does to first order approximate a multi-aperture antenna with three phase centers, where the impulse locations are the independent phase centers.

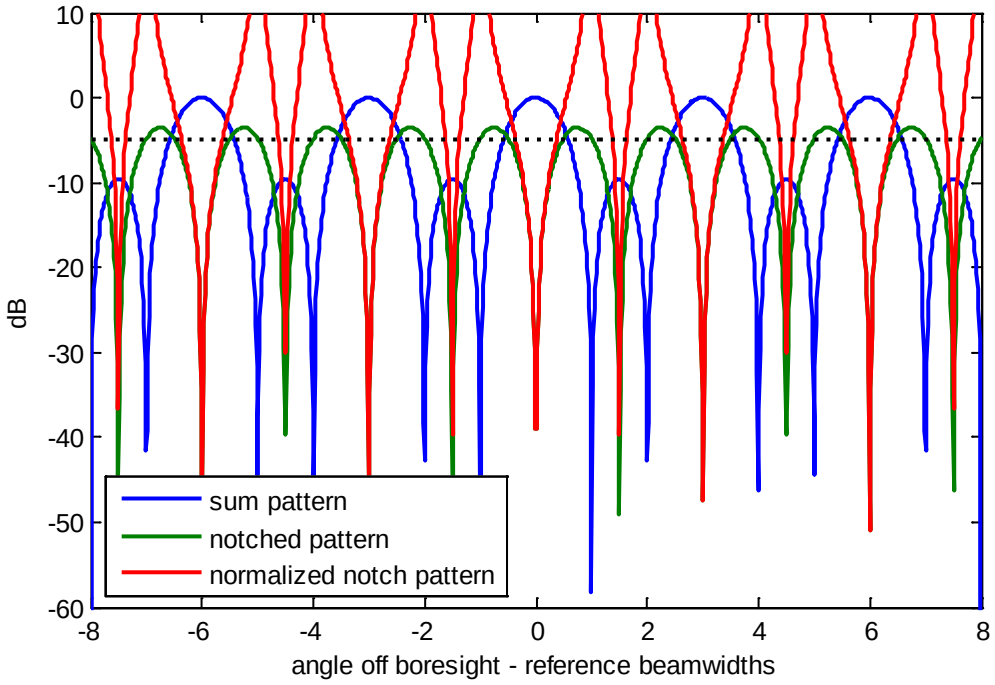


**Figure 18. The far-field pattern of a uniformly sampled aperture along with the notched pattern given by Eq. (47), and normalized notched pattern given by Eq. (48).**

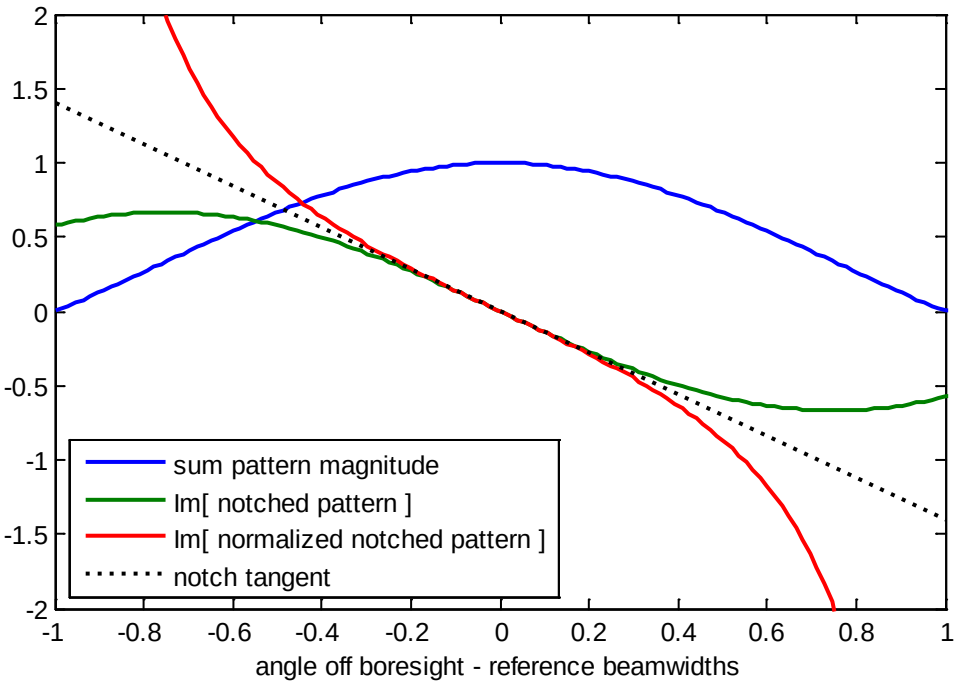


**Figure 19. The far-field patterns of Figure 18 plotted on a linear scale, and zoomed to the region of the mainlobe of the sum pattern.**

***Some Comments About the Monopulse Slope for Odd Number of Samples***

The normalized monopulse slope at the center of the beam pattern for the odd number of samples is in fact given by

$$slope = -\frac{\pi}{2}\left(1-\frac{1}{N^2}\right). \tag{49}$$

We observe that this is less than the $-(\pi/2)$ slope for all even numbers of samples, including for $N=2$. This seems to suggest that dividing the aperture into an odd number of samples is inherently inferior to dividing the same aperture into an even number of samples, owing to null being placed on the center sample of the delta channel aperture illumination function.

However, it is important to note that the monopulse slope is not the whole story. The real measure of performance is ultimately the accuracy and precision with which a DOA measurement can be made, i.e. the noise in the DOA measurement. This is addressed in Appendix A, and will be further discussed later in this report.

A sneak peak ahead, and at Appendix A, shows that DOA performance for $N=3$ actually is slightly improved over the case where $N$ is even, in spite of the less-steep monopulse slope.

# 6 Uniform Aperture Divided Into Subapertures

We now modify our design criteria for a notched antenna pattern to embody the following characteristics.

1. A true null with zero gain in a programmable (or processed) direction.
2. A 'notch' around the null that is of minimum width.
3. A gain in other directions that is as near to unity as possible within the neighborhood of the sum pattern mainlobe, subject to the constraint on the aperture illumination functions that they are a set of equally-spaced and equal-area uniformly illuminated subapertures.

$$\left|p_\Delta(x)\right| = \left|p_\Sigma(x)\right| = \sum_{n=0}^{N-1} \frac{1}{D}\,\mathrm{rect}\left(\frac{x - x_n}{D/N}\right), \tag{50}$$

except perhaps for the subaperture centered at $x = 0$. Here, $x_n$ are the centers of the subaperture positions in the overall aperture. In addition, while we have scaled the rect functions by $1/D$. This is for convenience and not essential to the significance of the results.

Here we also constrain that any one elemental position in the sum pattern aperture exhibits the same magnitude gain as the respective elemental position in the notched pattern aperture, except perhaps for the subaperture centered at $x = 0$. The phase between the two apertures may be significantly different. As before, we define the sample positions as

$$x_n = \frac{D}{N}n - \frac{D}{N}\left(\frac{N-1}{2}\right), \tag{51}$$

where the sample indexed positions are identified

$$n \in \textit{Integers}, \text{ where } 0 \le n < N. \tag{52}$$

Borrowing from the earlier analysis, we define the aperture illumination functions as

$$p_\Delta(x) = \frac{1}{N}\sum_{n=0}^{N-1} \mathrm{sgn}(x)\, e^{j2\pi\frac{\theta_0}{\lambda}x}\,\delta\left(x - \frac{D}{N}n + \frac{D}{N}\left(\frac{N-1}{2}\right)\right) * \frac{N}{D}\,\mathrm{rect}\left(\frac{x}{D/N}\right), \text{ and}$$

$$p_\Sigma(x) = \frac{1}{N}\sum_{n=0}^{N-1} e^{j2\pi\frac{\theta_0}{\lambda}x}\,\delta\left(x - \frac{D}{N}n + \frac{D}{N}\left(\frac{N-1}{2}\right)\right) * \frac{N}{D}\,\mathrm{rect}\left(\frac{x}{D/N}\right), \tag{53}$$

where "*" denotes convolution. Note that these are equal-length segments formed by dividing the larger aperture into subapertures. We have constructed these functions as

convolutions of the sample impulse functions from the previous sections. This will allow us to build on the earlier analysis. Accordingly, we identify the Fourier Transform pair

$$\frac{N}{D}\text{rect}\left(\frac{x}{D/N}\right) \Leftrightarrow \text{sinc}\left(\frac{D}{N}\left(\frac{\theta}{\lambda}\right)\right). \tag{54}$$

As before, for convenience, we will separately analyze the case of an even number of samples from the case of an odd number of samples.

## 6.1 Even Number of Samples

We now concern ourselves with only even values of *N*. We repeat and slightly expand the aperture illumination functions as

$$p_\Delta(x) = \left[\begin{array}{l} -\frac{1}{N}\sum_{n=0}^{N/2-1} e^{j2\pi\frac{\theta_0}{\lambda}x}\delta\left(x-\frac{D}{N}n+\frac{D}{N}\left(\frac{N-1}{2}\right)\right) \\ +\frac{1}{N}\sum_{n=N/2}^{N-1} e^{j2\pi\frac{\theta_0}{\lambda}x}\delta\left(x-\frac{D}{N}n+\frac{D}{N}\left(\frac{N-1}{2}\right)\right) \end{array}\right] * \frac{N}{D}\text{rect}\left(\frac{x}{D/N}\right), \text{ and}$$

$$p_\Sigma(x) = \frac{1}{N}\sum_{n=0}^{N-1} e^{j2\pi\frac{\theta_0}{\lambda}x}\delta\left(x-\frac{D}{N}n+\frac{D}{N}\left(\frac{N-1}{2}\right)\right) * \frac{N}{D}\text{rect}\left(\frac{x}{D/N}\right). \tag{55}$$

The corresponding antenna patterns can then be calculated in closed form as

$$P_\Delta\left(\frac{\theta}{\lambda}\right) = \frac{-j2}{N}\left(\frac{\sin^2\left(\pi\left(\frac{\theta-\theta_0}{\theta_{BW}}\right)\left(\frac{1}{2}\right)\right)}{\sin\left(\pi\left(\frac{\theta-\theta_0}{\theta_{BW}}\right)\left(\frac{1}{N}\right)\right)}\right)\text{sinc}\left(\frac{1}{N}\left(\frac{\theta}{\theta_{BW}}\right)\right),$$

$$= \frac{-j}{N}\left(\frac{1-\cos\left(\pi\left(\frac{\theta-\theta_0}{\theta_{BW}}\right)\right)}{\sin\left(\pi\left(\frac{\theta-\theta_0}{\theta_{BW}}\right)\left(\frac{1}{N}\right)\right)}\right)\text{sinc}\left(\frac{1}{N}\left(\frac{\theta}{\theta_{BW}}\right)\right),$$

and

$$P_\Sigma\left(\frac{\theta}{\lambda}\right) = \frac{1}{N}\left(\frac{\sin\left(\pi\left(\frac{\theta-\theta_0}{\theta_{BW}}\right)\right)}{\sin\left(\pi\left(\frac{\theta-\theta_0}{\theta_{BW}}\right)\left(\frac{1}{N}\right)\right)}\right)\text{sinc}\left(\frac{1}{N}\left(\frac{\theta}{\theta_{BW}}\right)\right). \tag{56}$$

The normalized pattern is then calculated as

$$P_{\Delta/\Sigma}\left(\frac{\theta}{\lambda}\right) = \frac{P_{\Delta}\left(\frac{\theta}{\lambda}\right)}{j\,P_{\Sigma}\left(\frac{\theta}{\lambda}\right)} = -\left(\frac{1-\cos\left(\pi\left(\frac{\theta-\theta_0}{\theta_{BW}}\right)\right)}{\sin\left(\pi\left(\frac{\theta-\theta_0}{\theta_{BW}}\right)\right)}\right). \tag{57}$$

The aperture illumination functions for $N = 4$ are illustrated in Figure 20. The corresponding antenna pattern plots are given in Figure 21 and Figure 22.

We make the following observations.

- The normalized notch pattern, as well as the notch pattern itself (scaled to equivalent gain and unit reference beamwidth), exhibits a normalized monopulse slope of $-(\pi/2)$ at the center of the sum pattern, in the vicinity of the null.
- This is essentially the same as the continuous uniform aperture.
- The −5 dB notch width is 0.83, with normalized notch width of 0.65.
- This aperture illumination function is quite realistic.

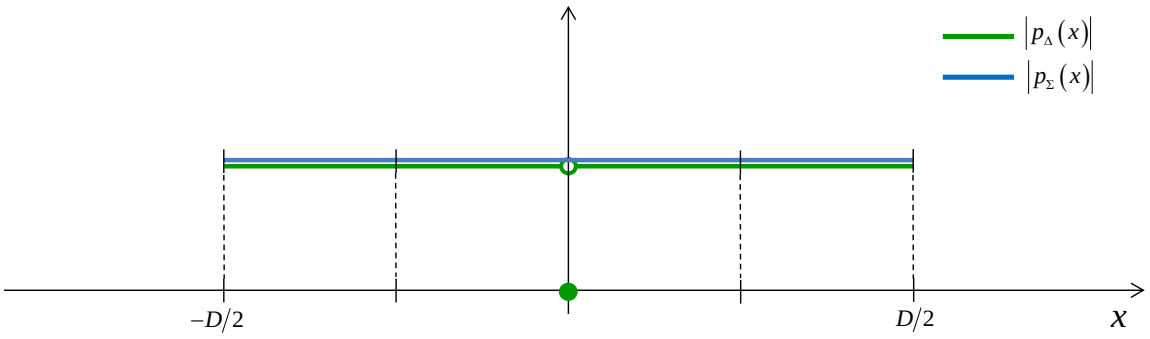


**Figure 20. Aperture illumination for uniform sampled delta and sum channels.**

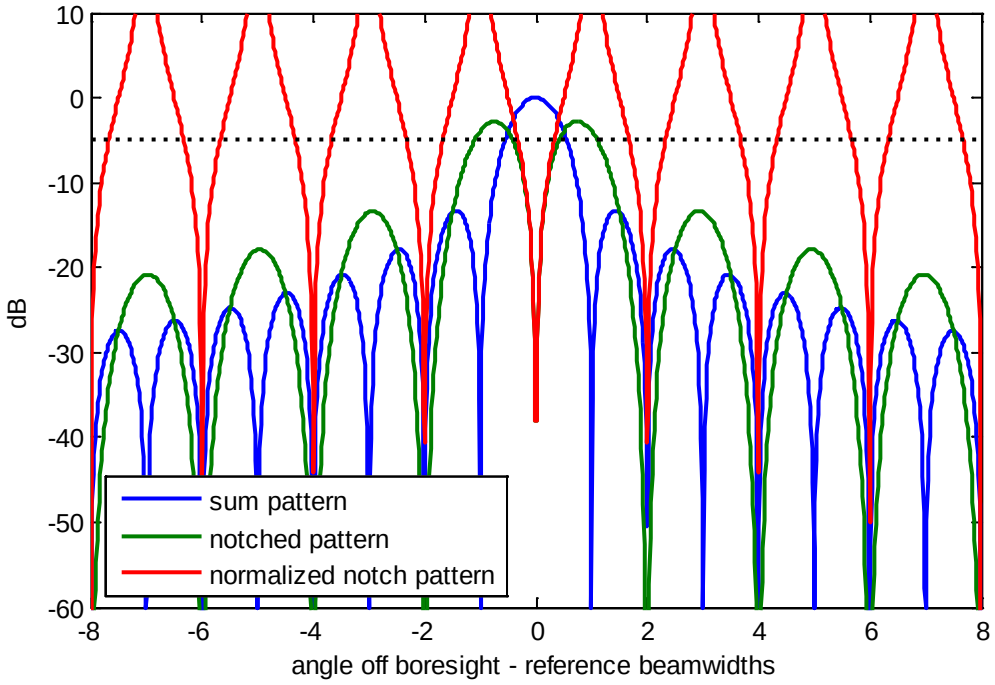


**Figure 21. The far-field pattern of uniform subaperture along with the notched pattern given by Eq. (56), and normalized notched pattern given by Eq. (57).**

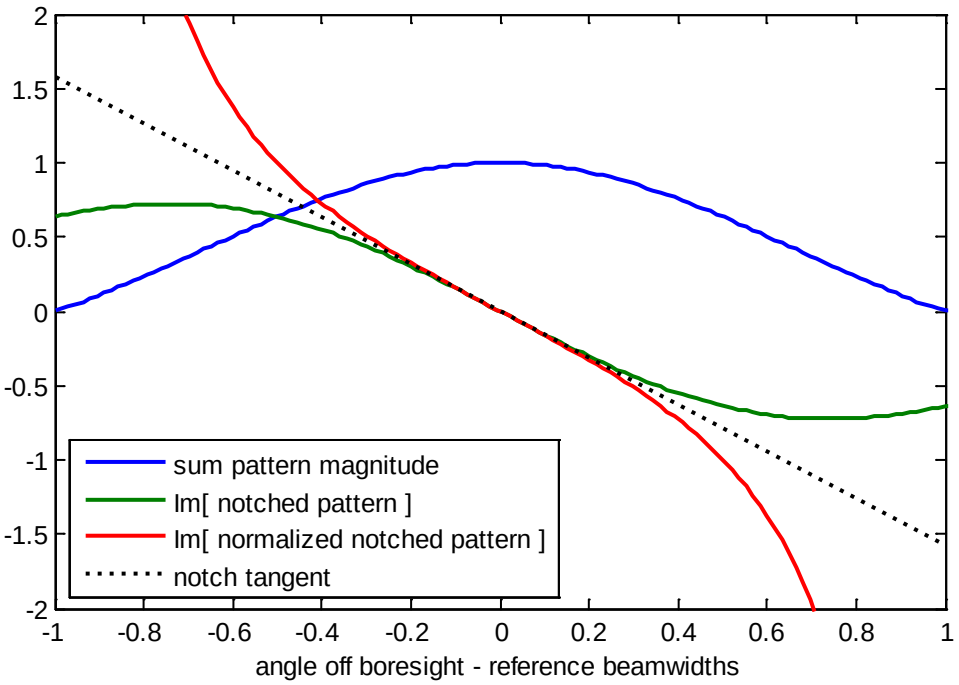


**Figure 22. The far-field patterns of Figure 21 plotted on a linear scale, and zoomed to the region of the mainlobe of the sum pattern.**

## 6.2 Odd Number of Samples

We now concern ourselves with only odd values of *N*. We note that with an odd number of subapertures, that the center subaperture falls at the center of the aperture, and will be nulled by the signum function in the notched pattern aperture illumination function. The sum pattern aperture illumination function analysis is otherwise unaffected by even versus odd number of samples, so we will repeat it here for completeness. Consequently, we repeat and slightly expand the aperture illumination functions as

$$p_{\Delta}(x)=\left[\begin{array}{l}-\frac{1}{N}\sum_{n=0}^{(N/2-3/2)}e^{j2\pi\frac{\theta_0}{\lambda}x}\delta\left(x-\frac{D}{N}n+\frac{D}{N}\left(\frac{N-1}{2}\right)\right)\\+\frac{1}{N}\sum_{n=(N/2+1/2)}^{N-1}e^{j2\pi\frac{\theta_0}{\lambda}x}\delta\left(x-\frac{D}{N}n+\frac{D}{N}\left(\frac{N-1}{2}\right)\right)\end{array}\right]*\frac{N}{D}\text{rect}\left(\frac{x}{D/N}\right),$$

and

$$p_{\Sigma}(x)=\frac{1}{N}\sum_{n=0}^{N-1}e^{j2\pi\frac{\theta_0}{\lambda}x}\delta\left(x-\frac{D}{N}n+\frac{D}{N}\left(\frac{N-1}{2}\right)\right)*\frac{N}{D}\text{rect}\left(\frac{x}{D/N}\right). \tag{58}$$

The corresponding closed-form antenna patterns can then be calculated as

$$P_{\Delta}\left(\frac{\theta}{\lambda}\right)=\frac{-j2}{N}\left(\frac{\begin{array}{l}\sin\left(\pi\left(\frac{\theta-\theta_0}{\theta_{BW}}\right)\left(\frac{N-1}{2N}\right)\right)\\\times\sin\left(\pi\left(\frac{\theta-\theta_0}{\theta_{BW}}\right)\left(\frac{N+1}{2N}\right)\right)\end{array}}{\sin\left(\pi\left(\frac{\theta-\theta_0}{\theta_{BW}}\right)\left(\frac{1}{N}\right)\right)}\right)\text{sinc}\left(\frac{1}{N}\left(\frac{\theta}{\theta_{BW}}\right)\right),$$

$$=\frac{-j}{N}\left(\frac{\cos\left(\pi\left(\frac{\theta-\theta_0}{\theta_{BW}}\right)\left(\frac{1}{N}\right)\right)-\cos\left(\pi\left(\frac{\theta-\theta_0}{\theta_{BW}}\right)\right)}{\sin\left(\pi\left(\frac{\theta-\theta_0}{\theta_{BW}}\right)\left(\frac{1}{N}\right)\right)}\right)\text{sinc}\left(\frac{1}{N}\left(\frac{\theta}{\theta_{BW}}\right)\right),$$

$$P_{\Sigma}\left(\frac{\theta}{\lambda}\right)=\frac{1}{N}\left(\frac{\sin\left(\pi\left(\frac{\theta-\theta_0}{\theta_{BW}}\right)\right)}{\sin\left(\pi\left(\frac{\theta-\theta_0}{\theta_{BW}}\right)\left(\frac{1}{N}\right)\right)}\right)\text{sinc}\left(\frac{1}{N}\left(\frac{\theta}{\theta_{BW}}\right)\right). \tag{59}$$

The normalized pattern is calculated as

$$P_{\Delta/\Sigma}\left(\frac{\theta}{\lambda}\right)=\frac{P_{\Delta}\left(\frac{\theta}{\lambda}\right)}{j\,P_{\Sigma}\left(\frac{\theta}{\lambda}\right)}=-\left(\frac{\cos\left(\pi\left(\frac{\theta-\theta_0}{\theta_{BW}}\right)\left(\frac{1}{N}\right)\right)-\cos\left(\pi\left(\frac{\theta-\theta_0}{\theta_{BW}}\right)\right)}{\sin\left(\pi\left(\frac{\theta-\theta_0}{\theta_{BW}}\right)\right)}\right). \tag{60}$$

The aperture illumination functions for $N=3$ are illustrated in Figure 23. The corresponding antenna pattern plots are given in Figure 24 and Figure 25.

We make the following observations.

- The notched pattern for an odd number of samples approaches that for an even number of samples as *N* increases.
- The normalized notch pattern, as well as the notch pattern itself (scaled to equivalent gain and unit reference beamwidth), exhibits a normalized monopulse slope of something less than $-(\pi/2)$ at the center of the sum pattern, in the vicinity of the null. This is because of the zeroed center subaperture due to the null at $x=0$.
- The –5 dB notch width is 1.04, with normalized notch width of 0.73.
- This aperture illumination function is quite realistic.

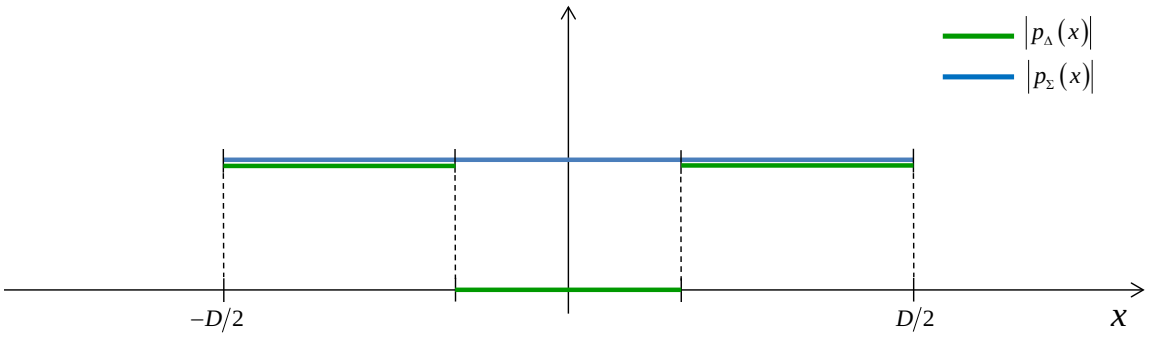


**Figure 23. Aperture illumination for uniform sampled delta and sum channels.**

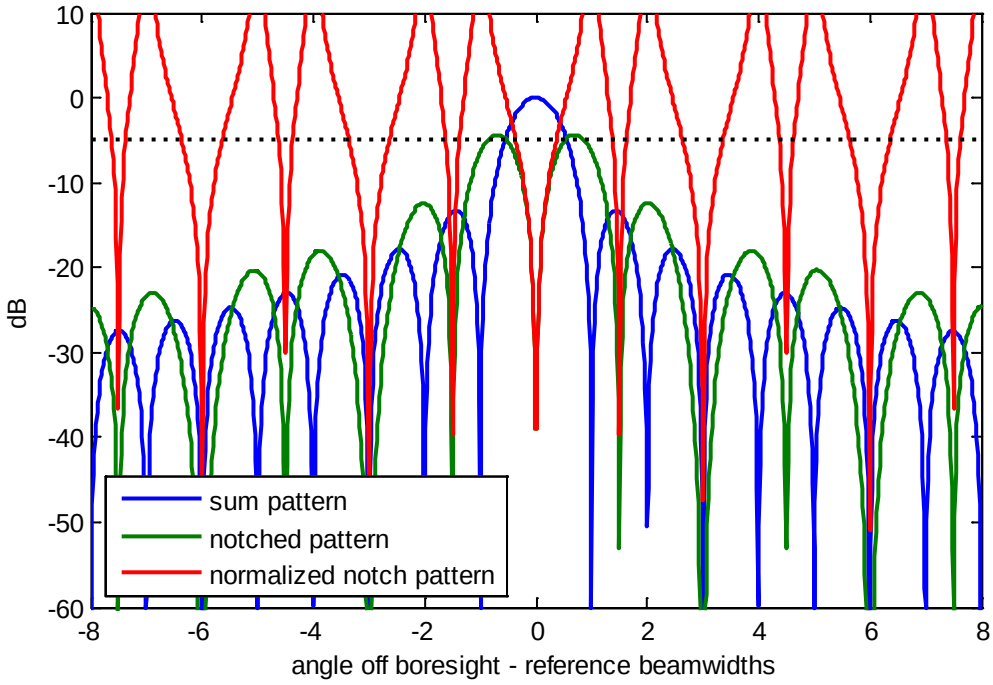


**Figure 24. The far-field pattern of a uniformly sampled aperture along with the notched pattern given by Eq. (59), and normalized notched pattern given by Eq. (60).**

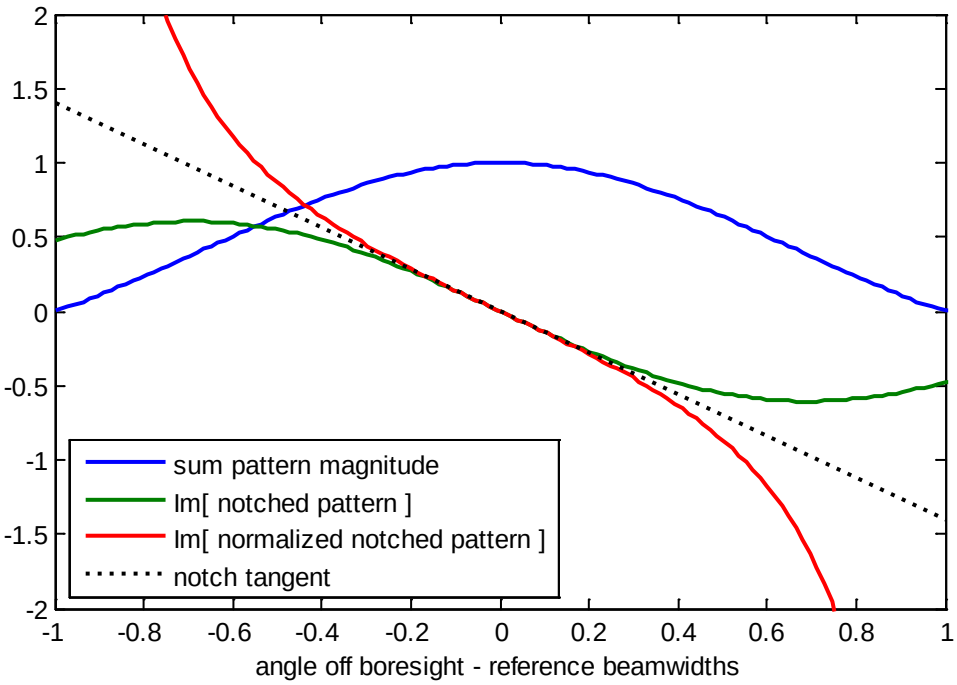


**Figure 25. The far-field patterns of Figure 24 plotted on a linear scale, and zoomed to the region of the mainlobe of the sum pattern.**

*“Learning isn't acquiring knowledge so much as it is trimming information that has already been acquired.” ― Criss Jami*

# 7 Miscellaneous Discussion

Here we address some miscellaneous questions, issues, and myths.

## 7.1 Monopulse Slope is Everything… Not Really

The notch width is directly related to monopulse slope, and the monopulse slope is certainly related to the noisiness of the DOA estimation. It is true that the noisiness of the DOA estimate is inversely proportional to monopulse slope if specific other parameters can be kept constant. However that is not to be expected.

One might ask "Why do we care about DOA estimation when we presume to know exactly the DOA of stationary clutter?"

The answer to this is that this DOA noise is the uncertainty of where the clutter signal actually appears, regardless of where we place the null to filter the clutter.

Nevertheless, one might be inclined to believe that the steeper the monopulse slope, the smaller our DOA noise, and the better would be our system performance. However, this takes too simplistic a view regarding noise.

We examine two cases.

***Case 1.***

Monopulse slope is a function of the baseline between antenna subaperture phase centers. However, although the noise in a DOA estimate (i.e. the noise that perturbs the DOA of a target or clutter) decreases for increasing baseline, if the baseline increase comes at a price of diminished overall aperture, then the DOA noise increase due to SNR loss will at times dominate. This is addressed in Appendix A. Consequently, it is quite possible that sometimes a steeper normalized monopulse slope will be accompanied with even noisier DOA estimates. In these cases, this is not a good trade.

***Case 2.***

Monopulse slope is proportional to the signal gain of the notched pattern's aperture. Simply scaling the signal from the aperture of the notched pattern relative to that of the sum would increase the monopulse slope. However DOA noise depends on SNR. Consequently, simply scaling the aperture's signal after the noise has been added will also scale its noise, and render the SNR unchanged. In this case a steeper normalized monopulse slope will not result in improved DOA performance. There is no benefit to system performance by simply scaling aperture signals.

## 7.2 Notch Width and Doppler Resolution

The question we now concern ourselves with is "How well can we expect a DOA notch to filter radar scene clutter?"

We begin by noting that in a focused range-Doppler map, clutter will occupy an individual resolution cell of nominal width that equals the angular resolution of the data. That is, the angular resolution of the clutter is

$$\rho_{DOA} = \frac{\lambda}{2T_{CPI} v_a \sin|\theta_s|} = \text{angular resolution of Doppler data,} \tag{61}$$

where

$T_{CPI}$ = coherent processing time interval,
$v_a$ = horizontal radar velocity,
$\theta_s$ = squint angle with respect to velocity vector, and
$\lambda$ = nominal wavelength of radar signal. (62)

To facilitate the following discussion, we zoom in on the notch displayed in Figure 21 and render it in Figure 26. From this figure, we measure the notch width at various attenuations with respect to the sum pattern peak response, and present them in Table 1.

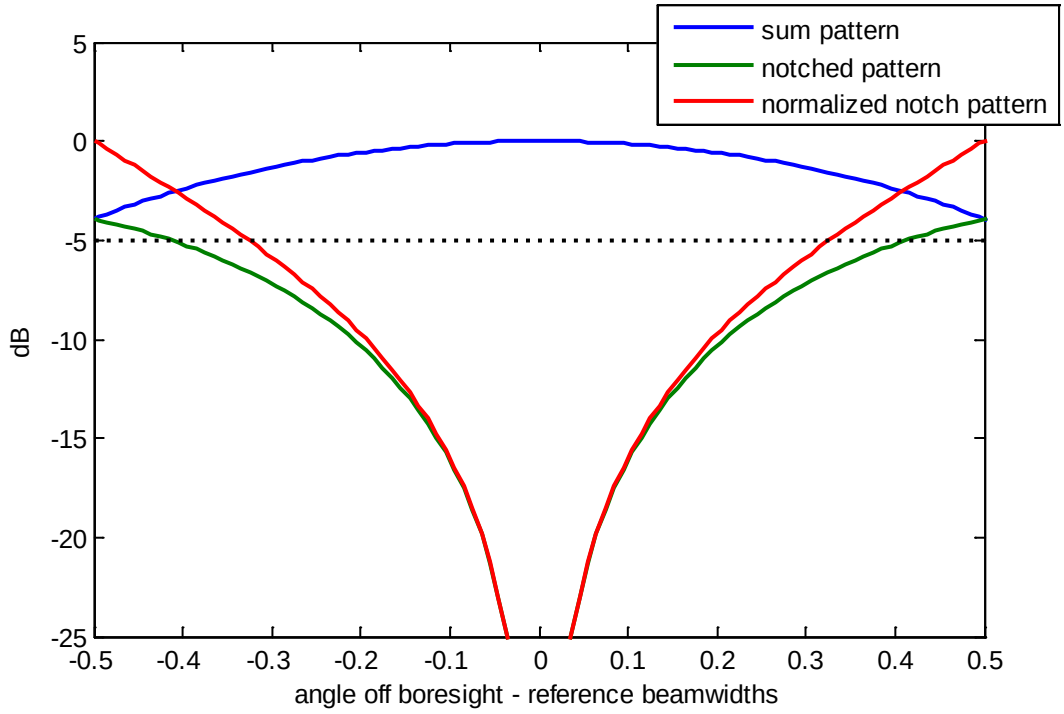


**Figure 26. Zoomed rendering of Figure 21.**

**Table 1. Notch width profile in fractions of nominal beamwidth.**

| Attenuation for Width | Notch Pattern | Normalized Notch Pattern |
|---|---|---|
| –5 dB | 0.83 | 0.65 |
| –10 dB | 0.42 | 0.39 |
| –20 dB | 0.13 | 0.13 |

Suppose now that for a given attenuation level the normalized notch width is defined as

$$\eta \text{ = normalized notch width.} \tag{63}$$

For example, $\eta$ takes on the values in Table 1 for the specified attenuation levels. Then, to achieve the required attenuation for all clutter within a particular range-Doppler resolution cell, we require

$$\rho_{DOA} \le \eta\, \theta_{BW} \ . \tag{64}$$

More explicitly, this may be expanded and rearranged to identify a limit on the notch width such that it exceeds the Doppler width of a clutter resolution cell as

$$\eta \ge \frac{\lambda}{2\theta_{BW} T_{CPI} v_a \sin|\theta_s|} \ . \tag{65}$$

This then tells us the achievable attenuation. We illustrate this with a pair of examples.

***Example 1***

Consider a radar operating with the parameters

$$\begin{aligned} &\theta_{BW} = 0.05 \ \text{(2.9 degrees)}, \\ &T_{CPI} = 0.1, \\ &v_a = 50 \text{ m/s}, \\ &\theta_s = \pi/4 \ \text{(45 degrees)}, \\ &\lambda = 0.018. \end{aligned} \tag{66}$$

The normalized notch width must then satisfy

$$\eta \ge 0.0509 \ . \tag{67}$$

With the apertures of Figure 26, this corresponds to clutter attenuation by at least 28 dB at the edge of the resolution cell.

***Example 2***

Now consider the previous example except with a more forward squint angle, namely

$$\theta_S = \pi/20 \quad (9 \text{ degrees}). \tag{68}$$

The normalized notch width must now satisfy

$$\eta \geq 0.2301 \; . \tag{69}$$

With the same apertures of Figure 26, this corresponds to clutter attenuation by not quite 15 dB at the edge of the resolution cell.

Essentially, as we move to examine DOA away from broadside, our ability to suppress clutter diminishes. More generally, as the clutter compresses into fewer Doppler resolution cells for whatever reason, our ability to cancel it with an antenna pattern null evaporates.

## 7.3 More Notch Width and Doppler Resolution

Here we present a more sophisticated model for discussing the notch width versus Doppler resolution. This model has a strong relationship to a phenomenon inherent to Interferometric Synthetic Aperture Radar (IFSAR or InSAR) as reported by Bickel, et al.,[7] and by Bickel,[8] but uses an array processing mathematical approach adapted from Zatman.[6]

We can define the appropriate notch width required for a given Doppler resolution cell with uniform clutter as the baseline separation that can be approximated as a *spatial* "narrowband" signal. Following the argument by Zatman, we will declare the notch width to be inadequate when the second largest eigenvalue of the spatial covariance matrix between channels is large enough. As in Zatman, we also say that this occurs when the second largest eigenvalue is larger than the noise (eigenvalue). What follows is the mathematics that defines this model.

Assume we have a uniform linear array (ULA) with characteristics

$$\begin{aligned} D &= \text{overall length of the array, and} \\ N &= \text{number of subapertures.} \end{aligned} \tag{70}$$

From this, we calculate the array spacing

$$d = D/N = \text{the separation between subaperture centers.} \tag{71}$$

Also, if we assume that the clutter is stationary (i.e., no so-called "internal clutter motion" for example due to wind), then the angular spread of the resolution should follow the previous Eq. (61). Under the assumption that the clutter is uniform across the resolution cell and following the method, the second eigenvalue of the spatial covariance matrix is given by

$$\lambda_2 = \left(\frac{cnr}{2}\right)\left(1-|\psi|\right). \tag{72}$$

where

$cnr$ = the Clutter-to-Noise Ratio (CNR) for the sum channel (unitless), (73)

and $\psi$ will be defined below.

For this development, instead of using Eq. (61), we will use the Doppler bandwidth, $\Delta f_D$, across the resolution cell as the inverse of the CPI time, namely

$$\Delta f_D = 1/T_{CPI}\ . \tag{74}$$

Then, defining the apparent phase difference between two pseudo-targets with the same statistics as the uniform clutter resolution cell as

$$\Delta\psi = \pi\left(\frac{\Delta f_D}{\sqrt{3}\sin|\theta_s|}\right)\left(\frac{d}{v_a}\right), \tag{75}$$

we now identify $|\psi|$ as

$$|\psi| = \left|\frac{\sin\left\{N\pi\left(\frac{\Delta f_D}{2\sqrt{3}\sin|\theta_s|}\right)\left(\frac{d}{v_a}\right)\right\}}{N\sin\left\{\pi\left(\frac{\Delta f_D}{2\sqrt{3}\sin|\theta_s|}\right)\left(\frac{d}{v_a}\right)\right\}}\right|, \tag{76}$$

or similarly,

$$|\psi| = \left|\frac{\sin\left\{\left(\frac{\pi}{2\sqrt{3}\sin|\theta_s|}\right)\left(\frac{Nd}{v_a T_{CPI}}\right)\right\}}{N\sin\left\{\left(\frac{\pi}{2\sqrt{3}\sin|\theta_s|}\right)\left(\frac{d}{v_a T_{CPI}}\right)\right\}}\right|. \tag{77}$$

We could further tweak Eq. (77) by recalling that $D = Nd$ and noting that

$$L_a = v_a T_{CPI} \text{ = length of the "synthetic aperture,"} \tag{78}$$

however we will choose not do so at this point. Note that Eq. (77) is the familiar Dirichlet function, also sometimes called the periodic sinc function, or aliased sinc function.

Finally, similar to Zatman, we desire the condition that the signal to be nulled is sufficiently narrow-band in Doppler that it can in fact be adequately nulled, i.e. attenuated to the noise level. This implies that we wish the second eigenvalue be adequately small, in fact, that the following condition is met,

$$\lambda_2 < 1. \tag{79}$$

Combining these equations yields the condition

$$\left(\frac{cnr}{2}\right)\left[1 - \left|\frac{\sin\left\{\left(\frac{\pi}{2\sqrt{3}\sin|\theta_s|}\right)\left(\frac{Nd}{v_a T_{CPI}}\right)\right\}}{N\sin\left\{\left(\frac{\pi}{2\sqrt{3}\sin|\theta_s|}\right)\left(\frac{d}{v_a T_{CPI}}\right)\right\}}\right|\right] < 1. \tag{80}$$

It is important to notice that this condition is a function of the CNR. Higher CNRs make this condition more difficult to meet.

The condition is also a function of the ratio of separations between the phase centers to the length of the "synthetic aperture". For those familiar with IFSAR, this latter result is not unfamiliar. The implication of this is that larger antennas require finer resolution. This matches our intuition that larger antennas result in narrower nulls which result in lower MDV, but which may be too narrow to adequately null out a coarse (wide) Doppler resolution cell. It should be emphasized that we are only considering spatial processing in this report. Belaboring the point, similar concepts have been shown for IFSAR.[8]

Eq. (79) can be rewritten in decibels as

$$CNR - 3.01 + 10\log_{10}\left[1 - \left|\frac{\sin\left\{\left(\frac{\pi}{2\sqrt{3}\sin|\theta_s|}\right)\left(\frac{Nd}{v_a T_{CPI}}\right)\right\}}{N\sin\left\{\left(\frac{\pi}{2\sqrt{3}\sin|\theta_s|}\right)\left(\frac{d}{v_a T_{CPI}}\right)\right\}}\right|\right] < 0 \text{ dB}, \tag{81}$$

where

$$CNR = 10\log_{10}\left(cnr\right) \text{ = CNR in dB.} \tag{82}$$

Some final transmogrifications yields the condition on *CNR* as

$$CNR < 3.01 - 10\log_{10}\left[1 - \left|\frac{\sin\left\{N\left(\frac{\pi}{2\sqrt{3}\sin|\theta_s|}\right)\left(\frac{d}{L_a}\right)\right\}}{N\sin\left\{\left(\frac{\pi}{2\sqrt{3}\sin|\theta_s|}\right)\left(\frac{d}{L_a}\right)\right\}}\right|\right] \text{ dB.} \tag{83}$$

This suggests that for a given ratio of $\left(d/L_a\right)$, there exists an upper bound on CNR. This also suggests that for a given CNR, that there is a constraint on the ratio $\left(d/L_a\right)$, also an upper bound.

***Example***

Assume we are imaging at broadside using two phase centers separated by $d$. The required ratio $\left(d/L_a\right)$ must be less than or equal to that shown in Figure 27 to adequately null the clutter in the resolution cell with a given CNR.

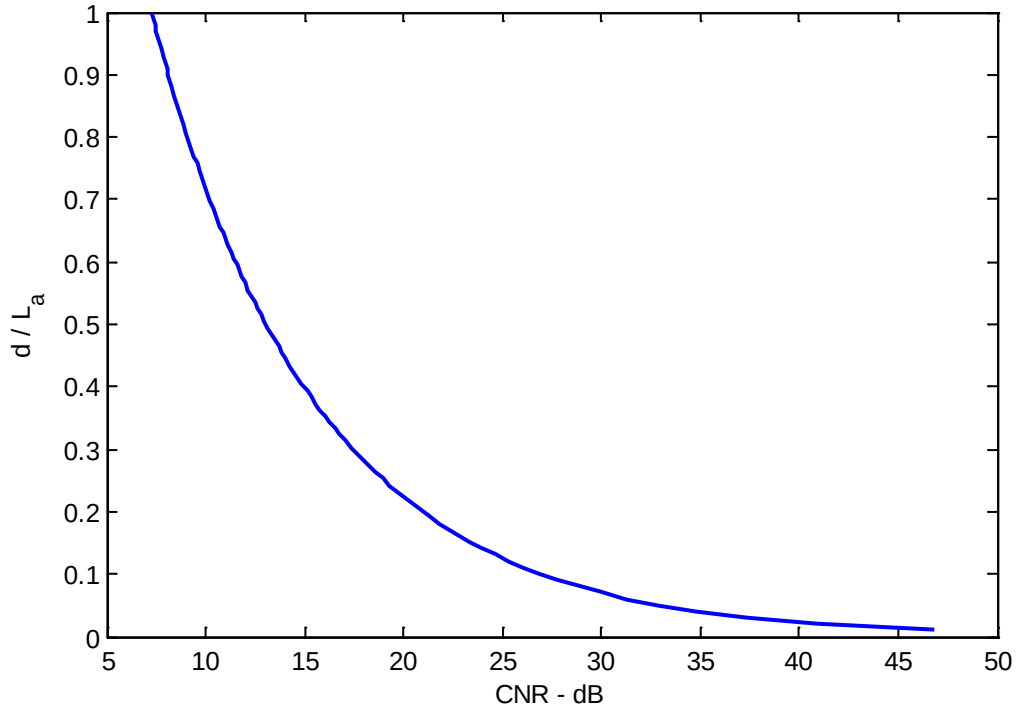


**Figure 27. Maximum $d/L_a$ ratio to meet the nulling condition for given CNR.**

## 7.4 Minimum Detectable Velocity

Perhaps no other descriptor of performance more dominates discussion of GMTI modes than Minimum Detectable Velocity (MDV). While strictly speaking we are quite capable of detecting targets even with zero velocity, what we really typically are interested in is "How slow can a moving target move in a line-of-sight direction, and still be discernable from stationary clutter?"

Neglecting issues of Doppler resolution as discussed in the previous section, we observe that a moving target exhibiting some Doppler frequency will be discernable from stationary clutter at the same Doppler frequency by its DOA departing the expected value for the stationary clutter. For slow-moving targets, the DOA difference is proportional to the target velocity. That is

$$v_t = v_a \sin\left|\theta_s\right| \theta_\Delta \quad = \text{target line-of-sight velocity,} \tag{84}$$

where

$$\theta_\Delta \quad = \text{DOA angle difference between target and clutter.} \tag{85}$$

We will assume for convenience that positive DOA angle differences correspond to positive Doppler shifts, which in turn correspond to positive line-of-sight target velocity.

We also define a normalized version of $\theta_\Delta$ as

$$\varphi_\Delta = \frac{\theta_\Delta}{\theta_{BW}} \quad = \text{normalized DOA angle difference between target and clutter.} \tag{86}$$

This normalized angle corresponds to the abscissa of the many far-field pattern plots given up to now in this report. Nevertheless, we may equate

$$v_t = v_a \sin\left|\theta_s\right| \theta_{BW}\ \varphi_\Delta\,. \tag{87}$$

Determining MDV is now the following sequence of tasks.

1. decide how much attenuation we are willing to tolerate in the normalized notch pattern,
2. determine the corresponding normalized DOA angle difference that yields that level of attenuation, and
3. calculating the corresponding target velocity via Eq. (85) and assign this to MDV.

While this procedure will supply an MDV number, we stipulate that it is quite possible to detect some targets at velocities significantly less than this number. Consequently, the MDV will be SNR (in the sum-channel) dependent. Among other things, this means that

MDV will be range-dependent. Details of how such an SNR may be calculated are given in a report by Doerry.[9]

We illustrate with a pair of examples.

***Example 1***

Consider a GMTI radar with the following operating parameters.

$$\begin{aligned} \theta_{BW} &= 0.05 \text{ (2.9 degrees)}, \\ v_a &= 50 \text{ m/s, and} \\ \theta_s &= \pi/4 \text{ (45 degrees).} \end{aligned} \tag{88}$$

Furthermore, let the radar exhibit notch characteristics as rendered in Figure 26, and operating with a noise floor with a noise-equivalent Radar Cross Section (RCS) of −30 dBsm. Let us assume a detection criteria of at least 15 dB of SNR after clutter cancellation.

Now consider a target representative of a dismount with RCS of −10 dBsm. Consequently, to detect this target we may tolerate only 5 dB of loss by the clutter filter. This suggests an allowable $\varphi_\Delta$ of 0.325, which corresponds to an MDV of 0.57 m/s.

***Example 2***

Consider the same radar as the previous example, but now a target exhibiting an RCS of +5 dBsm. To detect this target we may tolerate 20 dB of loss by the clutter filter. This suggests an allowable $\varphi_\Delta$ of 0.065, which corresponds to an MDV of 0.11 m/s.

*“Bottom line is, if you do not use it or need it, it's clutter, and it needs to go.”*
*— Charisse Ward*

# 8 Conclusions

We summarize several points herein as follows.

- Multi-aperture or multi-subaperture antennas are fundamental to high-performance GMTI systems, where targets need to be detected when their range-Doppler response has similar characteristics to background clutter.

- Multiple phase centers can be used to cancel stationary clutter, so as to discriminate slow moving targets. An important question is "How well can multiple subapertures cancel clutter, and let moving target energy still pass?"

- Real antennas have constraints on their physical extent. The overall antenna width places a fundamental limit on the notch width use to cancel clutter.

- More subapertures will not necessarily yield better performance, either in target detectability, or DOA performance *against a single target*.

- Monopulse slope is directly related to notch width.

- In general a larger monopulse slope is better, but not always. DOA noise is related to monopulse slope, but not exclusively so. Sometimes monopulse slope can be sacrificed for better (lower) DOA noise.

- For good clutter cancellation, the angular width of a Doppler resolution cell must be small compared to the notch width. Consequently, clutter cancellation becomes less effective as the radar squints away from broadside.

- The Minimum Detectable Velocity for multiple subaperture antennas is a function of SNR in the sum beam. Consequently, the MDV will depend on, among other things, target RCS and range.

- We further stipulate that phase center separation sets monopulse slope vs. subaperture dimension that sets grating lobes vs. subaperture taper that sets subaperture array factor. In addition, a linear phase ramp across (and between) subapertures steers the beam.

*"When you have cleared all of your clutter,*
*you can be of greater service to those around you."*
*— Michael B. Kitson*

# Appendix A – Direction of Arrival Noise

We herein examine several issues regarding the noise in a Direction of Arrival (DOA) estimate. Accordingly, we build on a paper by Doerry and Bickel.[10] The underlying equation for the subsequent analysis is the familiar expression

$$\sigma_{DOA} = \frac{\lambda}{2\pi b_{eff}\sqrt{SNR}}, \tag{89}$$

where

$\lambda$ = nominal wavelength,
$b_{eff}$ = the effective baseline between antenna phase centers, and
$SNR$ = signal power/energy to noise power/energy ratio. (90)

A tacit assumption here is that the SNR is for a single image due to one phase center in the interferometer.

## Trading Aperture for Baseline

Consider an antenna that has available to it an aperture of width $D$, but divides it into two uniform subapertures with geometry as illustrated in Figure 28.

Accordingly we define

$D$ = the available global antenna aperture length of the receive antenna, and
$\alpha$ = fractional width of individual subapertures. (91)

Furthermore, we assign the individual subapertures to be equal to each other, except separated in location.

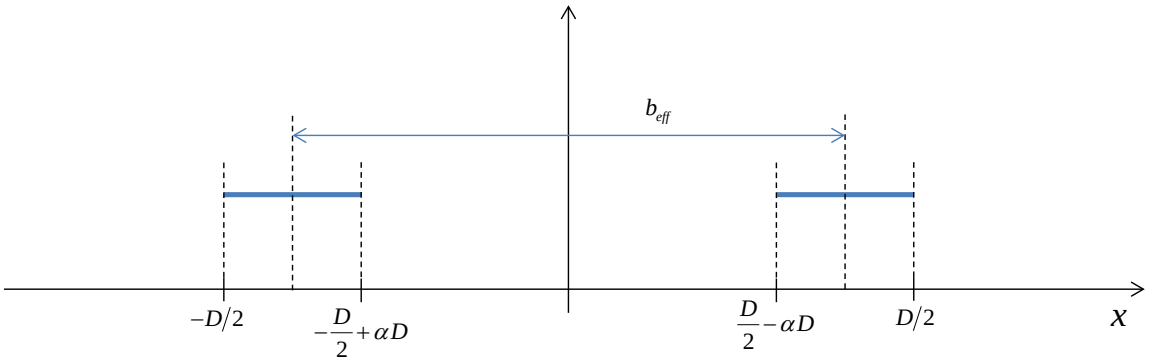


**Figure 28. Geometry of aperture relating to baseline.**

Accordingly, we identify the subaperture as

$$D_{subap} = \alpha D \text{ = the aperture length of a subaperture.} \tag{92}$$

We may then identify the RMS noise in a DOA measurement with the expression

$$\sigma_{DOA} = \frac{C_1}{b_{eff}\sqrt{D_{subap}}}, \tag{93}$$

where

$$C_1 \text{ = constant of proportionality that involves other radar parameters.} \tag{94}$$

and the baseline separating the nominal subaperture positions as

$$b_{eff} = D - D_{subap} = D(1-\alpha). \tag{95}$$

Combining these into the DOA RMS noise expression yields

$$\sigma_{DOA} = \frac{C_1}{D(1-\alpha)\sqrt{\alpha D}} = \frac{1}{\left[(1-\alpha)\sqrt{\alpha}\right]}\left(\frac{C_1}{D^{3/2}}\right). \tag{96}$$

We observe that the term in the square brackets of Eq.(94) can be interpreted as a figure of merit, with better performance for larger values. That is

$$\chi = (1-\alpha)\sqrt{\alpha} \text{ = Figure of Merit for DOA noise versus subaperture width.} \tag{97}$$

We plot this in Figure 29, and note that a clear maximum exists at $\alpha = 1/3$. This clearly shows that for our geometry of Figure 28, the minimum DOA noise is achieved when $\alpha = 1/3$. In this case, the gap between subaperture edges is equal to the individual subaperture widths.

It is also instructive to plot the equivalent SNR increase that this figure of merit represents with respect to the case where $\alpha = 1/2$. We do this in Figure 30, and note that the advantage of $\alpha = 1/3$ is worth only a small fraction of a dB, over the case $\alpha = 1/2$.

This yields an important observation, namely

- For a constrained pair of subapertures, an optimum is achieved by balancing the effects of baseline with the effects of subaperture widths. Increasing/decreasing baseline at the expense decreasing/increasing subaperture length will cause a net increase in DOA noise. This is undesirable.

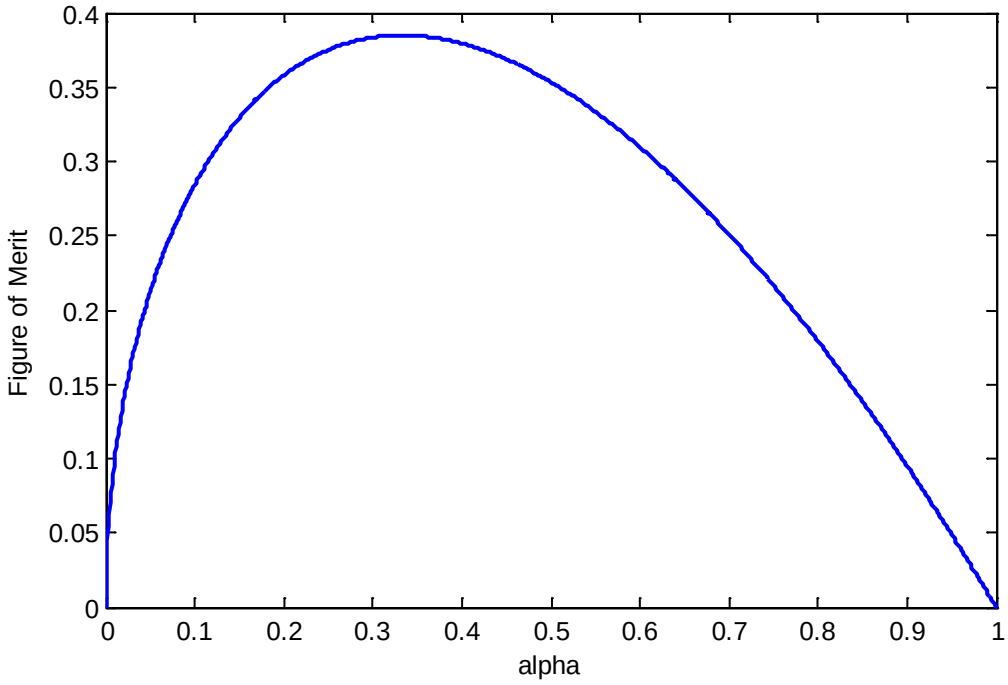


**Figure 29. Figure of merit for subaperture size.**

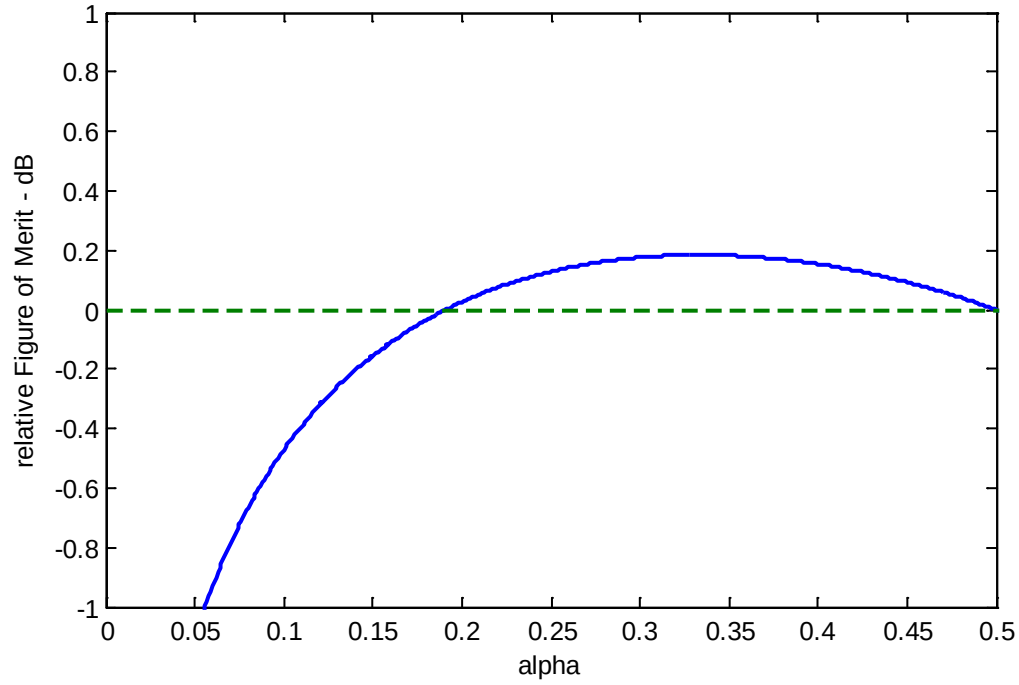


**Figure 30. Plot of Figure 29 in dB relative to $\alpha = 1/2$.**

***Example 1***

In particular, consider the case where we let

$$\alpha = (N-1)/(2N), \tag{98}$$

for odd integer values of *N*. In this case, our figure of merit becomes

$$\chi = (1-\alpha)\sqrt{\alpha} = \left(1-\frac{(N-1)}{(2N)}\right)\sqrt{\frac{(N-1)}{(2N)}}. \tag{99}$$

More importantly, $\chi$ is maximized, and DOA noise is minimized, when $\alpha = 1/3$, that is, when $N = 3$.

For this case $N = 3$, the improvement is equivalent to about 0.18 dB of SNR improvement, or about a 9% baseline increase, compared to the case where $N = 2$. Interestingly, although the actual baseline increased by 33%, the reduction in SNR due to smaller apertures limits the sensitivity to as if the baseline were increased by only 9%, but it is still an increase.

## Monopulse Slope and Noise

We return to the RMS noise in an interferometric DOA measurement described by the expression

$$\sigma_{DOA} = \frac{\lambda}{2\pi b_{eff}\sqrt{SNR}}, \tag{100}$$

and recall that the SNR was for both transmitting and receiving on a subaperture.

The actual angle calculation is given by

$$\theta = \frac{\lambda}{2\pi b_{eff}}\Delta\phi \text{ = DOA angle estimate,} \tag{101}$$

where

$$\Delta\phi \text{ = phase difference measured at ends of baseline } \theta = b_{eff}. \tag{102}$$

We now further identify

$b'_{eff} = \dfrac{b_{eff}}{D}$ = effective baseline normalized to antenna aperture length, and

$\theta_{BW} = \dfrac{\lambda}{D}$ = nominal sum pattern beamwidth. (103)

This allows us to write the normalized DOA angle as

$$\frac{\theta}{\theta_{BW}} = \frac{1}{2\pi b'_{eff}}\Delta\phi \text{ = normalized DOA angle estimate.} \quad (104)$$

Now we turn our attention to the measured phase difference $\Delta\phi$, and recognize it as the expression

$$\Delta\phi = \text{atan}\left(\frac{\text{Im}\left(P_\Sigma(\theta/\lambda) - P_\Delta(\theta/\lambda)\right)}{\text{Re}\left(P_\Sigma(\theta/\lambda) - P_\Delta(\theta/\lambda)\right)}\right) - \text{atan}\left(\frac{\text{Im}\left(P_\Sigma(\theta/\lambda) + P_\Delta(\theta/\lambda)\right)}{\text{Re}\left(P_\Sigma(\theta/\lambda) + P_\Delta(\theta/\lambda)\right)}\right), \quad (105)$$

where

$P_\Sigma(\theta/\lambda)$ = sum antenna pattern, and

$P_\Delta(\theta/\lambda)$ = notched antenna pattern. (106)

We have constructed the interferometer such that a negative measured phase difference corresponds to a positive DOA. Furthermore, we will assume that no additional phase slope is applied across the apertures to steer the beam away from its nominal broadside direction. From the main body of this report, for real $P_\Sigma(\theta/\lambda)$ and imaginary $P_\Delta(\theta/\lambda)$, the phase difference then reduces to

$$\Delta\phi = \text{atan}\left(\frac{-P_\Delta(\theta/\lambda)}{jP_\Sigma(\theta/\lambda)}\right) - \text{atan}\left(\frac{P_\Delta(\theta/\lambda)}{jP_\Sigma(\theta/\lambda)}\right) = -2\,\text{atan}\left(\frac{P_\Delta(\theta/\lambda)}{jP_\Sigma(\theta/\lambda)}\right), \quad (107)$$

which may be written more compactly as

$$\Delta\phi = -2\,\text{atan}\left(P_{\Delta/\Sigma}(\theta/\lambda)\right). \quad (108)$$

For small angles (i.e. near the sum-beam center) this can be approximated as

$$\Delta\phi \approx -2P_{\Delta/\Sigma}(\theta/\lambda). \quad (109)$$

The factor of two in this expression is why such a phase-comparison monopulse radar is sometimes called a “half-angle tracker.”

Nevertheless, this lets us write the normalized DOA estimate as

$$\frac{\theta}{\theta_{BW}} = \frac{-1}{\pi b'_{eff}} P_{\Delta/\Sigma}\left(\theta/\lambda\right) . \tag{110}$$

We now define the normalized monopulse slope as

$$m_{MP} = \lim_{\theta \to 0}\left(\frac{P_{\Delta/\Sigma}\left(\theta/\lambda\right)}{\theta/\theta_{BW}}\right) = -\pi\, b'_{eff} \text{ = normalized monopulse slope.} \tag{111}$$

This allows us to write the normalized DOA estimate as

$$\frac{\theta}{\theta_{BW}} = \frac{1}{m_{MP}} P_{\Delta/\Sigma}\left(\theta/\lambda\right) . \tag{112}$$

This in turn also allows us to write the DOA noise expression as

$$\sigma_{DOA} = \frac{\lambda}{2m_{MP}\sqrt{SNR}} . \tag{113}$$

It is essential to observe that the monopulse slope is a measure of baseline only, and consequently is not the whole story when it comes to DOA estimation noise.

***Example 2***

In particular, consider the case where we let

$$b'_{eff} = 1/2 . \tag{114}$$

This is equivalent to a sampled uniform aperture with $N = 2$. From this we may calculate

$$m_{MP} = -\frac{\pi}{2} . \tag{115}$$

This is consistent with the analysis for a sampled uniform aperture where the actual slope at the center of the sum beam was calculated to be $-\left(\pi/2\right)$.

# Reference


[1] Armin W. Doerry, Douglas L. Bickel, "GMTI Direction of Arrival Measurements from Multiple Phase Centers," Sandia Report SAND2015-2310, Unlimited Release, March 2015.

[2] Samuel M. Sherman, *Monopulse Principles and Techniques*, ISBN 0-89006-137-8, Artech House, 1984.

[3] Samuel M. Sherman, David K. Barton, *Monopulse Principles and Techniques – second edition*, ISBN-13 978-1-60807-174-6, Artech House, 2011.

[4] *IEEE Standard Radar Definitions*, IEEE Std 686™-2008, Sponsored by the Radar Systems Panel, IEEE Aerospace and Electronic Systems Society, 21 May 2008.

[5] William L. Melvin, "Space-Time Detection Theory," ADP014040, Paper presented at the RTO SET Lecture Series on "Military Application of Space-Time Adaptive Processing"' held in Istanbul, Turkey, 16-17 September 2002, Wachtberg, Germany, 19-20 September 2002, Moscow, Russia, 23-24 September 2002, and published in RTO-EN-027.

[6] M. Zatman, "How narrow is narrowband?, " *IEE Proceedings Radar, Sonar and Navigation*, Volume 145, Issue 2, pp. 85-91, April 1998.

[7] D. L. Bickel, D. A. Yocky, W. H. Hensley "The effect of scattering from buildings on interferometric SAR measurements," IGARSS'97, Vol. 4, pp. 1545 – 1547, Singapore, 3-8 Aug 1997.

[8] D. L. Bickel, "A null-steering viewpoint of interferometric SAR," IGARSS'00, Vol. 7, pp. 3206 - 3209, Honolulu, HI, 24-28 Jul, 2000.

[9] Armin W. Doerry, "Performance Limits for Exo-Clutter Ground Moving Target Indicator (GMTI) Radar", Sandia Report SAND2010-5844, Unlimited Release, September 2010.

[10] A. W. Doerry, D. L. Bickel, "A comparison of interferometric SAR antenna options", SPIE 2013 Defense, Security & Sensing Symposium, Radar Sensor Technology XVII, Vol. 8714, Baltimore MD, 29 April – 3 May 2013.

# Distribution

Unlimited Release

| | | | | |
|---|---|---|---|---|
| 1 | MS 0532 | J. J. Hudgens | 5340 | |
| 1 | MS 0519 | J. A. Ruffner | 5349 | |
| 1 | MS 0519 | A. W. Doerry | 5349 | |
| 1 | MS 0519 | L. Klein | 5349 | |
| 1 | MS 0519 | D. L. Bickel | 5344 | |
| 1 | MS 0899 | Technical Library | 9536 | (electronic copy) |

Sandia National Laboratories